Original Article

Neu5Gc-associated Serum Immunoglobulin G Glycosylation as a Diagnostic Biomarker for Hepatocellular Carcinoma

Xu Cao[1,2#], Xiwei Lu[2#], Qingwei Li[1], Jiali Lu[1], Xiaoping Song[3], Yinglun Han[1], Chunwen Pu[2*] and Yue Pang[1*]

[1]Lamprey Research Center, College of Life Science, Liaoning Normal University, Dalian, Liaoning, China; [2]Dalian Municipal Research Institute for Public Health, Dalian Public Health Clinical Center, Dalian, Liaoning, China; [3]Respiratory Medicine, Affiliated Zhong Shan Hospital of Dalian University, Dalian, Liaoning, China

Abstract

Background and Aims: Given the lack of efficient biomarkers for hepatocellular carcinoma (HCC) diagnosis, this study aimed to develop an HCC diagnostic strategy based on serum protein glycosylation signatures. We characterized differential N-glycosylation patterns of serum IgG to differentiate HCC from healthy controls and liver cirrhosis, and elucidated the molecular mechanisms driving aberrant Neu5Gc elevation in HCC to provide a theoretical basis for clinical application and differential diagnosis of HCC. ***Methods:*** LIP-ELISA was applied to quantify serum Neu5Gc in 6,768 healthy individuals for baseline establishment. IgG was purified and subsequently analyzed by RPLC-MS/MS for glycosylation profiling in HCC and healthy samples. Bioinformatic analysis of *CMAH* and related gene clusters modulating Neu5Gc synthesis was conducted. ***Results:*** In a cohort of 1,114 participants, the LIP-ELISA platform achieved 80.21% sensitivity, 96.01% specificity, and 92.46% accuracy for primary HCC diagnosis. Serum IgG from HCC patients displayed multibranched N-glycans modified with core fucose and Neu5Gc. Key molecules involved in glycan modification were identified, enabling the development of multiplexed gene detection for HCC, LC, and chronic hepatitis B. *In vitro* assays confirmed hypoxia-induced sialic acid accumulation in HCC cells. Meanwhile, *CMAH*-knockout mouse experiments verified that an exogenous high-sialic-acid diet compensates for endogenous Neu5Gc synthesis deficiency, revealing a dietary-mediated compensatory mechanism for Neu5Gc elevation. ***Conclusions:*** This study established an LIP-ELISA-based clinical diagnostic platform combining AFP and Neu5Gc, defined sialic acid–modified glycan structures, and preliminarily identified regulators of Neu5Gc biosynthesis, providing novel insights for HCC diagnosis and mechanism research.

Citation of this article: Cao X, Lu X, Li Q, Lu J, Song X, Han Y, *et al*. Neu5Gc-associated Serum Immunoglobulin G Glycosylation as a Diagnostic Biomarker for Hepatocellular Carcinoma. J Clin Transl Hepatol 2026. doi: 10.14218/JCTH.2025.00654.

Introduction

Hepatocellular carcinoma (HCC) is a major global health challenge.[1] Current diagnostic markers, such as alpha-fetoprotein (AFP), and imaging techniques, such as ultrasonography, lack sufficient accuracy for reliable screening.[2] The Agile 3+ score, a simple noninvasive model that integrates liver stiffness measurement, serum biomarkers (AST, ALT, and platelet count), and clinical parameters (age, sex, and diabetes status), has been proposed for identifying advanced fibrosis in patients with suspected nonalcoholic fatty liver disease.[3,4] However, its diagnostic performance in patients with HCC remains insufficiently investigated, underscoring the need for complementary biomarkers for HCC detection, as explored in this study. Large-scale prospective cohort studies with longitudinally collected blood samples stored in biobanks offer a promising approach for the discovery of HCC biomarkers.

Glycosylation is a key post-translational modification that enhances functional diversity.[5] Aberrant glycosylation is a hallmark of various diseases, including cancer, and it can be used for disease diagnosis, staging, and potential therapeutic targeting.[6] It plays a vital role in protein synthesis as well as in lipid and drug metabolism in humans.[7] For example, monitoring the serum levels of oncofetal glycoproteins in patients with chronic liver disease is crucial for tracking progression to cirrhosis and HCC.[8] The predominant forms of sialic acids in mammals are N-acetylneuraminic acid (Neu5Ac) and N-glycolylneuraminic acid (Neu5Gc).[9] Humans do not synthesize Neu5Gc because of irreversible inactivation of the *CMAH* gene on chromosome 6p21.32, which encodes cytidine monophosphate–N-acetylneuraminic acid hydroxylase,[10] and the absence of an active monooxygenase resulting from exon deletions or mutations that cause frameshifts in *CMAH*.[11,12] Abnormal sialylation is often characterized by increased sialic acid levels on the cell surface. This not only elevates total sialic acid levels but also significantly alters the sialylation patterns of glycoproteins.[13] Moreover, Neu5Gc preferentially accumulates in malignant tissues, leading to elevated levels of Neu5Gc-modified proteins in tumors.[14–16]

Our laboratory identified a novel lamprey immune protein

(LIP) with lectin activity that specifically recognizes α2,3- or α2,6-glycosidic linkages of Neu5Gc-modified termini.[17,18] Although Neu5Gc is not synthesized in healthy humans owing to the absence of the *cmah* gene, elevated levels of Neu5Gc-modified proteins are detectable in various tumor cells and tissues.[19–21] N-glycan structures associated with Neu5Gc modification in patients with HCC have not been systematically analyzed. This study provides a theoretical foundation for the clinical development of tumor diagnostic markers and tumor-specific therapeutic targets and sheds light on the mechanisms underlying the abnormal Neu5Gc distribution on tumor cell surfaces.

Methods

Grouping and inclusion criteria

This study was approved by the Ethics Committees of Dalian Public Health Clinical Center (No. 2021-016-002), Affiliated Zhongshan Hospital of Dalian University (No. 2021053-1), and Liaoning Normal University (No. LL2020015) and was conducted from January 2020 to June 2022 in accordance with the Declaration of Helsinki (2024 revision).[22] A total of 8,791 participants were enrolled, comprising a training cohort (n = 8,043) and a validation cohort (n = 748). The training cohort included 144 patients with chronic hepatitis B (CHB), 144 with chronic hepatitis C (CHC), 192 with liver cirrhosis (LC), 634 with HCC, 6,768 healthy individuals, and 203 postoperative samples. The validation cohort included 98 patients with CHB, 103 with LC, 192 with HCC, and 355 healthy individuals. All participants provided written informed consent. Participants were required to be at least 18 years old with no prior hepatitis treatment. Exclusion criteria were pregnancy, acute HBV infection, HIV coinfection, and chronic alcohol use. Chronic HBV infection was defined as HBsAg positivity for >6 months with elevated HBeAg status, ALT, or AST.[23] LC was diagnosed based on ultrasonography, hypoalbuminemia, and prolonged prothrombin time.[24] Patients with liver stiffness measurements obtained by transient elastography (FibroScan; Echosens, Paris, France) ≥14.6 kPa were preferentially included. HCC was diagnosed using ultrasonography or computed tomography of the liver masses and an AFP level of 400 ng/mL.[25]

Study participants and recruitment

This was a multi-center, cross-sectional study. Healthy participants were consecutively enrolled from physical examinations of faculty, staff, and freshmen at Liaoning Normal University (2021–2022). Patients with HCC, LC, and chronic hepatitis were consecutively recruited from Dalian Public Health Clinical Center and Zhongshan Hospital Affiliated of Dalian University. Strict inclusion and exclusion criteria were applied to exclude individuals with other malignancies, severe systemic diseases, or incomplete clinical data.

At Dalian Public Health Clinical Center, eligible patients were identified from the institutional biobank using standardized diagnostic criteria. All serum samples were stored under uniform conditions, labeled with QR codes and unique anonymous identifiers, and dispatched to the laboratory without group information. Laboratory personnel were blinded to clinical diagnoses during all testing procedures. Group assignments were only unlocked after completion of all laboratory analyses. Study subjects were recruited from Affiliated Zhongshan Hospital of Dalian University. Samples were collected and coded before laboratory testing and data documentation. Clinical information and patient grouping status were provided monthly by clinical physicians.

The validation set was assessed in two independent blinded phases: first, samples were tested blindly using QR codes; second, random samples were re-coded and retested blindly by independent laboratory investigators, with results cross-verified against final discharge diagnoses. For healthy participants, samples were coded by the university hospital before testing; individuals with persistently abnormal Neu5Gc levels were excluded after medical record review. All data were regularly cross-verified against electronic medical records to ensure diagnostic accuracy and minimize information bias.

LIP enzyme-linked immunosorbent assay (ELISA)

A standard lectin ELISA was performed following a previously described protocol,[26] with modifications for serum versus urine sample handling, requiring post-dilution testing of serum samples. Serum samples were diluted 1:100, and 40 μL was coated onto a 96-well plate and incubated overnight at 4 °C. The following day, the plate was washed once with TBST, and a 1:9 dilution of 10X Carbo-Free Blocking Solution (VECTOR, Newark, CA, USA) was added for blocking at 37 °C for 2 h. After removing the blocking solution, LIP-biotin was added and incubated at 37 °C for 3 h. The wells were then washed thrice with TBST. This was followed by incubation with streptavidin at 37 °C for 1 h and four additional washes with TBST. TMB substrate solution was added for color development (5–8 min), and a stop solution was applied. Optical density was measured using an ELISA reader. LIP-biotin was purified and labeled using an IgG calibration protein and TMB chromogenic solution (Solarbio, Beijing, China).[27]

Lectin blot assay

The lectin blot procedure is similar to Western blotting but involves lectin-glycan binding rather than antigen-antibody interaction.[28] Signal amplification relies on biotin-lectin recognition, which is detected on a PVDF membrane using enhanced chemiluminescence. Blood samples were diluted fivefold with physiological saline, denatured, subjected to electrophoresis, and transferred to a PVDF membrane. The membrane was fixed with acetone for 5–10 min, air-dried, baked at 60 °C for 20 min, and activated with methanol to enable LIP-biotin binding, followed by standard enhanced chemiluminescence imaging.[29,30]

Nano-liquid chromatography chip quadrupole time-of-flight mass spectrometry (nano-LC–Q-TOF MS)

The Coomassie-stained gel band corresponding to the LIP-biotin-identified protein was trypsin-digested for nano-LC–Q-TOF MS.[31,32] Nano-RPLC was performed using mobile phase A (0.1% formic acid and 5% acetonitrile in water) on a C18 pre-column (100 μm × 3 cm, 3 μm, 150 Å) at 2 μL/min. This was followed by an 8-min desalting step using an Eksigent NanoLC-Ultra™ system (AB SCIEX LLC, Hong Kong, China).

An analytical C18 reversed-phase column (75 μm × 15 cm, 3 μm, 120 Å) was used with a 10-min gradient from 5% to 40% mobile phase B (0.1% formic acid and 95% acetonitrile in water). Mass spectrometry (MS) was conducted using a Triple TOF 5600+ system (AB SCIEX) with a Nanospray III ion source. The spray voltage was set at 2.3 kV, and curtain gas, nebulizer gas, and source temperature were maintained at 30, 14, and 150 °C, respectively. Data acquisition was performed in the information-dependent acquisition mode. A full-scan TOF-MS was performed at 250 ms, followed by up to 26 MS/MS scans per cycle for precursor ions (charge states 2+ to 5+, minimum intensity 200 cps). Each MS/MS scan had an accumulation time of 80 ms, with a total cycle time of 2.5 s. A constant collision energy was used, and a 3-s

dynamic exclusion was applied to avoid repeated ion sampling.[33]

Quantitative N-glycoproteomics using stable isotopic diethyl labeling

Serum IgG glycoproteins from patients with HCC and healthy participants were analyzed using quantitative N-glycoproteomics with stable isotopic diethyl labeling to obtain comprehensive data on N-glycosylation modifications (see Supplementary Information for details).[34] Proteins were reduced with 10 mM TCEP (CAS: 51805-45-9) at 55 °C for 1 h, alkylated with 20 mM iodoacetamide (IAA; CAS: 144-48-9) at room temperature (20–25 °C) for 30 min in the dark, and digested with trypsin at a 1:50 (w/w) ratio at 37 °C for 16 h.[35] The digests were desalted using C18 SPE tips and eluted with 50% and 80% acetonitrile containing 0.1% trifluoroacetic acid. The eluates were combined and dried using a SpeedVac concentrator. Intact N-glycopeptides were enriched using ZIC-HILIC SPE tips,[36] labeled by reductive diethylation with acetaldehyde and acetaldehyde-13C2, desalted, and dried for LC-MS analysis. For C18-RPLC-MS/MS (higher-energy collisional dissociation; HCD) analysis, a C18 analytical column (75 µm × 75 cm, 5 µm) and trap column (200 µm × 5 cm, 5 µm) were used. The flow rates were 5 µL/min for loading and 300 nL/min for analysis. The gradient was: 2% B for 12 min, 2%–40% B in 188 min, 40%–95% B in 10 min, 95% B for 5 min, and equilibration for 20 min. The ion transfer tube was maintained at 300 °C, with a spray voltage of 1.9 kV. The MS spectra were acquired from m/z 700–2,000 at a resolution of 60,000. The AGC target was 3×10^6 with a 20 ms maximum injection time. MS/MS spectra were acquired at a resolution of 30,000 using the Top20 DDA method with HCD and stepped NCEs (20%, 30%, and 31%). The AGC target was 5×10^5 with a 250 ms maximum injection time, an isolation window of 3.0 m/z, and a dynamic exclusion time of 20 s.[37]

Western blot (WB) and immunohistochemical staining

CMAH antibody (sc-365023, Santa Cruz, CA, USA) was used at a concentration of 0.3 µg/mL. The other antibodies (HIF-1α (D123654), VEGF (D360788), and GLUT1 (D160433)) were purchased from Sangon Biotech (Shanghai, China), and lectins (AAL [B-1395-1] and SNA [B-1305-2]) were purchased from Vector (USA). WB and immunohistochemical staining were performed according to standard protocols,[38,39] with the recommended concentrations of antibodies/lectins used in this study.

Nested polymerase chain reaction (PCR)

Two pairs of *CMAH* gene primers were designed to obtain full-length transcripts from the human genome using NCBI data. The first primer pair was positioned at the 5' and 3' ends of the gene to amplify the entire *CMAH* transcript, resulting in a longer product. The second primer pair was designed to flank the functional domain and yield a shorter amplification product. PCR amplification was initially performed using the first primer pair targeting the larger fragment for 40 cycles. Subsequently, the amplified products were subjected to a second round of PCR using shorter-fragment primers, following established nested PCR protocols.[40]

Flow cytometry and imaging flow cytometry

Cells were incubated with Alexa Fluor 488-labeled LIP (Thermo Fisher Scientific, catalog #A30006) for 10 min, followed by washing with PBS to remove unbound proteins. The cells were then stained with propidium iodide (Thermo Fisher Scientific, catalog #R37169) at room temperature for 15 min, collected, centrifuged at 1,000 rpm for 5 min, resuspended in 500 µL of PBS, and analyzed by flow cytometry.[41] The LIP, labeled with Alexa Fluor 488, was incubated with cells and subsequently detected by flow cytometry and fluorescence confocal microscopy. As the detection did not involve an antigen-antibody reaction, no isotype control antibodies were used. Instead, a positive control containing another commercial lectin, SNA, was used. The results were validated when SNA recognition matched the recognition pattern of LIP.[42]

Immunofluorescence detection of Neu5Gc on the cell surface

Cells were seeded in a four-chamber confocal dish (NEST, catalog #801002) at approximately 500 µL of cell suspension per well. After cell adhesion, the indicated drugs were added for co-incubation at specified time points, followed by replacement of the culture medium with fresh medium. LIP (0.2 µg/µL) was added and incubated for 2 h. Subsequently, a LIP monoclonal antibody, diluted 1:500 from an initial concentration of 1 µg/µL, was added and incubated for another 2 h. After washing with PBS, fluorescent secondary antibody (Thermo Fisher Scientific, catalog #A-11029, RRID: AB_2534088) was applied for 30 min. Fluorescence was detected using confocal microscopy following standard immunofluorescence protocols.[43]

Induction of isotopic glycans and sample collection for metabolomic analysis

Culture media were prepared according to the specific requirements of the cell lines. To eliminate Neu5Gc, human serum was used instead of fetal bovine serum, and cells were cultured in this medium for two to three passages. After more than 10 days of culture, Neu5Gc expression was undetectable using flow cytometry. Subsequently, 30 mM C13-labeled UDP-GlcNAc isotope was added, and the cells were incubated. Samples were collected at various time points, with the procedure involving flash-freezing the cells in liquid nitrogen, scraping them into microtubes, flash-freezing again, and storing at −80 °C.[44]

Non-targeted metabolomics detection

Initially, 500 µL of the extract was added to the sample, followed by two cycles of freezing in liquid nitrogen for 1 min, thawing, and vortexing for 30 s. The samples were then ultrasonicated in an ice water bath for 10 min and kept at −4 °C for 1 h. Subsequently, they were centrifuged at 13,800 × g at 4 °C for 15 min, and the supernatant was collected for analysis.[45] The data obtained were due to isotope labeling of the substrate, which allowed for the identification of metabolites containing different carbon isotopes in various pathways. The analysis focused on C13-labeled intermediate metabolites, with predictions based on time-series data and the sequence of metabolic steps. Further refinement of the experiment can be achieved through metabolic flux analysis.[46]

Quantitative reverse-transcription PCR (qRT-PCR)

As described in previous studies, cells were lysed in RNAex Pro Reagent (AG21102, Accurate Biotechnology, Changsha, China) to extract RNA. The extracted RNA was then reverse-transcribed into cDNA using the Evo M-MLV RT Kit with gDNA Clean for qPCR II (AG11705, Accurate Biotechnology, Changsha, China). qRT-PCR was performed in 20 µL reaction volumes using TB Green® Fast qPCR Mix (AG11701, Accurate
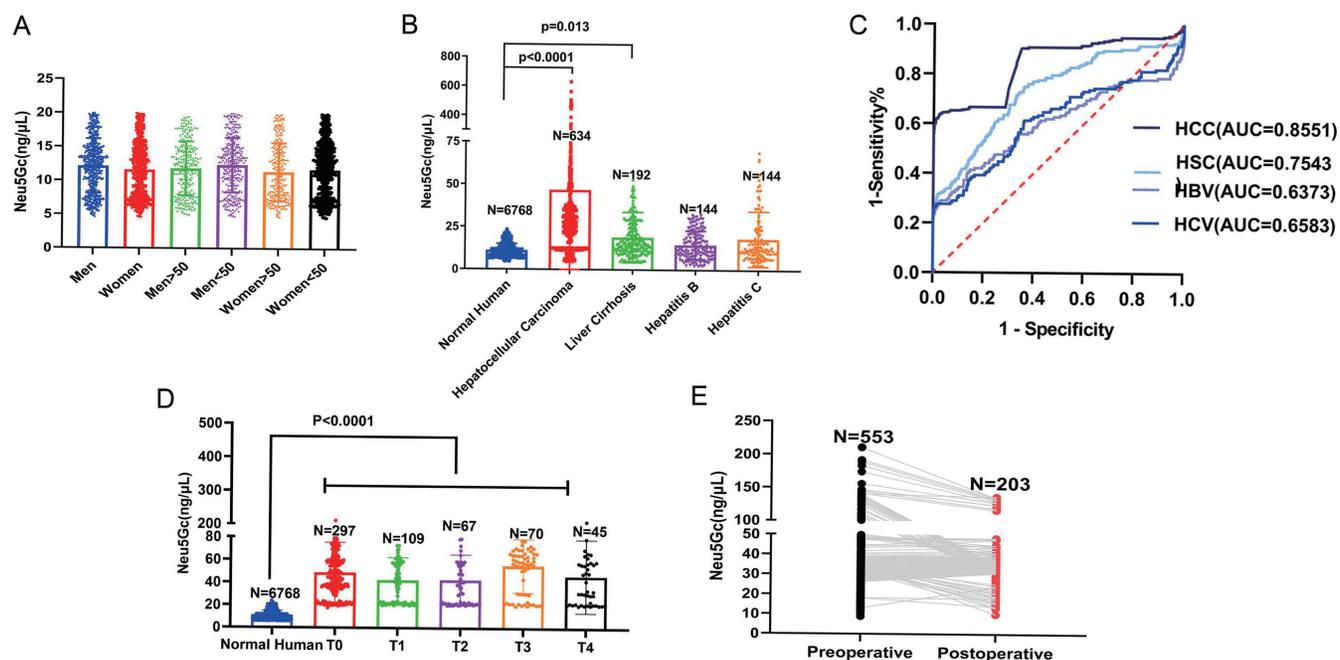
Fig. 1. Neu5Gc in the serum of various populations. Neu5Gc-glycoproteins in the serum were determined using LIP-ELISA. (A) Serum levels of Neu5Gc in healthy subjects according to age and sex. (B) Levels of the LIP-positive sialylated N-glycan Neu5Gc-terminal biomarker in the serum of healthy subjects and in patients with HCC, LC, CHB, and CHC. The number of samples per group is shown in parentheses. (C) ROC curves of LIP-positive sialylated N-glycan Neu5Gc-terminal biomarker panels for HCC, LC, CHB, and CHC patient groups versus healthy subjects, with the corresponding AUC and 95% CI. (D) Serum Neu5Gc glycoprotein levels in patients with different TNM stages in the HCC samples. (E) Differences in the content of sialylated N-glycan Neu5Gc termini in the serum of patients with HCC after different courses of treatment using ELISA. Data are expressed as scatter plots with bars (Wilcoxon Rank-Sum test). Neu5Gc, N-glycolylneuraminic acid; LIP, lamprey immune protein; HCC, hepatocellular carcinoma; LC, liver cirrhosis; CHB, chronic hepatitis B; CHC, chronic hepatitis C; AUC, area under the curve; CI, confidence interval; ELISA, enzyme-linked immunosorbent assay.

Biotechnology, Changsha, China), following standard qRT-PCR protocols.[47] The details of the primers used are provided in Supplementary Table 1.

Study design and statistical analysis

This analysis was conducted in accordance with the reporting recommendations for tumor marker prognostic studies.[48] Statistical analysis was performed using GraphPad Prism 8.0 (GraphPad). The diagnostic values of N-glycans and AFP were evaluated using a receiver operating characteristic (ROC) curve. The ROC cut-off (also called MID ROC) was the best threshold based on the ROC analysis. Diagnostic case-control studies were performed using the area under the ROC curve (AUC). Statistical significance was set at $P < 0.05$.[49,50] Multivariate linear regression for the combined analysis of AFP and Neu5Gc was performed using R Software (Version 3.5.3).[51]

Results

Diagnostic value of detecting Neu5Gc in serum by LIP-ELISA for HCC

Previous studies demonstrated that LIP could recognize the N-glycosylated terminal Neu5Gc modification of the uromodulin protein in urine, aiding in the early diagnosis of bladder cancer.[21] To explore the potential of Neu5Gc as a serum tumor biomarker detected by LIP, a prospective training cohort study was conducted using residual serum samples from routine physical examinations for faculty, staff, and incoming freshmen at Liaoning Normal University, with approval from the institutional ethics committee and broad informed con-

sent obtained from all participants prior to sample collection. Serum Neu5Gc levels in healthy individuals aged 18–105 years were analyzed according to age and sex. Given the higher incidence of HCC in individuals over 50 years of age, stratification was performed based on age (Fig. 1A), with further comparisons made at 10-year intervals for men (Supplementary Fig. 1A) and women (Supplementary Fig. 1B). Our data showed no statistically significant differences in Neu5Gc levels across the different age groups, with a mean serum Neu5Gc level of 10.81 ng/µL in healthy subjects.

From 2015 to 2022, blood samples were collected from patients diagnosed with CHB (n = 144), CHC (n = 144), LC (n = 192), and HCC (n = 634) and analyzed using LIP-ELISA (Fig. 1B). The mean Neu5Gc levels (C_{Neu5Gc}) in each group were: CHB, 14.46 ng/µL; CHC, 14.87 ng/µL; LC, 18.26 ng/µL; and HCC, 46.74 ng/µL. Diagnostic performance was systematically evaluated by ROC curve analysis for each disease group versus healthy controls, with complete ROC parameters as follows (Fig. 1C): HCC vs. healthy controls: AUC = 0.8551, standard error (SE) = 0.01894, 95% confidence interval (CI) = 0.8188–0.8915, $P < 0.0001$; LC vs. healthy controls: AUC = 0.7543, SE = 0.01953, 95% CI = 0.7160–0.7926, $P < 0.0001$; CHB vs. healthy controls: AUC = 0.6373, SE = 0.02873, 95% CI = 0.5810–0.6930, $P < 0.0001$; CHC vs. healthy controls: AUC = 0.6583, SE = 0.02671, 95% CI = 0.6059–0.7106, $P < 0.0001$. As the maximum likelihood ratio (Youden's index)[52] method failed to yield a cut-off with concurrent sensitivity and specificity >80%, the optimal serum Neu5Gc cut-off was determined as 22.85 ng/µL using the *top-left closest point method* (minimizing Euclidean distance to the perfect diagnostic point (0,1)), a gold-standard strategy for balancing clinical sensitivity and specificity.[53,54]

At this cut-off value, the key diagnostic indices for HCC identification were: sensitivity = 80.21%, specificity = 96.01%, positive predictive value = 89.74%, negative predictive value = 93.18%, and overall diagnostic accuracy = 92.46%. The previously reported specificity of 99.94% corresponded to a high-specificity subthreshold of the ROC curve, which was unsuitable for general HCC screening.

Further analysis of 588 samples according to tumor, node, and metastasis staging revealed that most cases were in the T0–T2 stages, which is consistent with the typical distribution pattern of tumor markers in early cancer screening.[55,56] Serum Neu5Gc levels in patients with HCC were significantly higher than those in healthy participants across different stages (Fig. 1D). Our method of using LIP to detect Neu5Gc effectively identified HCC samples with abnormally elevated Neu5Gc levels. To assess the therapeutic implications of serum Neu5Gc levels, we analyzed samples from untreated patients (Fig. 1E and Supplementary Fig. 1C), those who had undergone fewer than three cycles of chemotherapy post-HCC surgery, and those who had completed more than three cycles. We found that Neu5Gc levels correlated with treatment status, suggesting its potential use as an indicator of therapeutic efficacy. Therefore, our detection method offers a novel biomarker for the clinical diagnosis of HCC and serves as a surrogate marker for evaluating the effectiveness of HCC treatment.

Identification of Neu5Gc-modified glycoprotein in serum and its combination with AFP for diagnosis

The primary Neu5Gc-modified glycoproteins in serum recognized by LIP were analyzed using the LIP-biotin-based lectin-Western blot (LIP-WB) method. The corresponding bands were subjected to enzymatic digestion on Coomassie-stained gels, followed by MS identification (Supplementary Fig. 2A). Proteomic analysis was performed using nano-LC–Q-TOF MS, and MS/MS spectra were searched using Sequest within Proteome Discoverer (Thermo Fisher) against the UniProt *Homo sapiens* IgG database (Supplementary Fig. 2B). The main Neu5Gc-modified molecule identified was IgG glycoprotein.

To validate the accuracy of the LIP-identified targets in serum, samples were collected from newly admitted patients between 2020 and 2022 to establish a validation cohort. A total of 748 samples were collected: 355 from healthy subjects and 192, 103, and 98 from patients with HCC, LC, and CHB, respectively. Notably, the full cohort of 634 HCC samples was simultaneously assigned for subsequent AFP diagnostic performance analysis. However, 42 samples were excluded due to the lack of both definite tumor staging and liver fibrosis data. For healthy controls, 7,211 samples were tested. Among them, 443 samples with extremely abnormal indices were excluded, and 3,994 of the remaining 6,768 samples with available AFP detection values were screened for subsequent combined statistical analysis. Changes in serum IgG glycosylated proteins were assessed using sandwich LIP-ELISA (Supplementary Fig. 2C), in which plates were pre-coated with an IgG antibody. The results showed that the content of Neu5Gc-modified proteins was significantly higher in the HCC group than in the other groups (Fig. 2A), with serum Neu5Gc levels in HCC patients approximately sevenfold higher than those in healthy individuals, and an AUC of 0.8559 in the validation cohort (Fig. 2B), consistent with direct serum Neu5Gc detection. The IgG protein was digested with N-glucosidase to remove all N-glycan modifications. As shown in Supplementary Figure 2D, the molecular weight of the sample decreased after enzymatic digestion. Before enzyme digestion, the sample could be recognized by LIP, but after enzyme digestion, it could not be recognized by LIP-biotin, indicating that the recognition site of LIP was directly related to N-glycosylation. The correlation with O-glycosylation modification was verified by an O-glycosidase digestion experiment (Supplementary Fig. 2E), indicating that relatively few sugar chains are present on O-glycosylation-modified IgG, which has little influence on molecular weight. After N-glucosidase digestion, the samples from each group were titrated using ITC with LIP (Supplementary Fig. 2F and G). The results showed no binding between LIP and IgG after N-glucosidase digestion in any group. These findings confirmed that LIP primarily recognizes N-glycosylated terminal Neu5Gc modifications of IgG proteins in serum.

To identify additional biomarkers for HCC diagnosis in combination with Neu5Gc, we analyzed AFP levels (Fig. 2C) using the clinical standard of C_{AFP} >20 ng/mL. Among the 592 samples in the retrospective cohort (with clinical AFP measurements), 152 of the HCC samples met the diagnostic cut-off, resulting in a sensitivity of 25.67%. For a higher AFP threshold (C_{AFP} >400 ng/mL),[57,58] only 20 samples met the criteria, with a sensitivity of 3.3%. Interestingly, 36 AFP-positive samples exhibited low levels of Neu5Gc-modified proteins. Of the 440 AFP-negative HCC samples (AFP ≤ 20 ng/mL), 332 had Neu5Gc levels > 22.85 ng/μL. Parallel combined detection of AFP and Neu5Gc (defined as positive if either marker was above its cut-off) was further applied, achieving a sensitivity of 81.69%, specificity of 96.02%, and overall diagnostic accuracy of 94.64% for HCC. Multivariate linear regression analysis was additionally performed using R Software (Version 3.5.3) to quantify the combined effect: the regression equation was $y = 1.8926 + 0.0024X_1$ (AFP) + $43.1077X_2$ (Neu5Gc), with an R^2 of 0.7016 (70.2% explanatory power). AFP showed no significant independent effect ($P = 0.0822$), while Neu5Gc presented a significant positive independent association with the diagnostic outcome ($P < 0.05$). Thus, the combined use of LIP-detected Neu5Gc and AFP assays offers an effective dual-index diagnostic method (Fig. 2D and Table 1), which is particularly useful for screening HCC patients with low AFP levels. This dual approach significantly enhanced the sensitivity of HCC diagnosis.

Characteristics of N-glycosylation and differences in glycan composition detection and expression alterations of glycan-related genes between healthy subjects and HCC

To further elucidate the differences in N-linked glycosylation of IgG between healthy subjects and those with HCC, we employed C18-reversed-phase liquid chromatography coupled with tandem mass spectrometry (C18-RPLC-MS/MS) using HCD to comprehensively characterize the N-glycan structures. This approach enabled the detection of differences in glycosylation modifications and potential biomarkers. Glycomic mass spectrometric analysis was conducted on the purified IgG protein, and the main workflow is depicted in Supplementary Figure 3A. Examples of molecular weight prediction and B/Y ion matching for specific monosaccharide and glycan structures are shown in Supplementary Figure 3B.

Subsequent analysis of glycopeptides meeting the criteria of a fold change > 1.5 and $P < 0.05$ identified a total of 244 glycopeptides. A volcano plot (Fig. 3A) illustrates the upregulation and downregulation of these glycopeptides, revealing that 220 glycopeptides were significantly elevated (indicated in red), whereas 24 were decreased (indicated in blue). Overall, the N-glycan modifications in the HCC group showed a ninefold increase compared to those in healthy subjects. The distribution of N-glycan types, including high-mannose (4%), hybrid (11%), and complex (85%), is presented in Figure 3B. As depicted in Supplementary Figure 3C, the cleavage
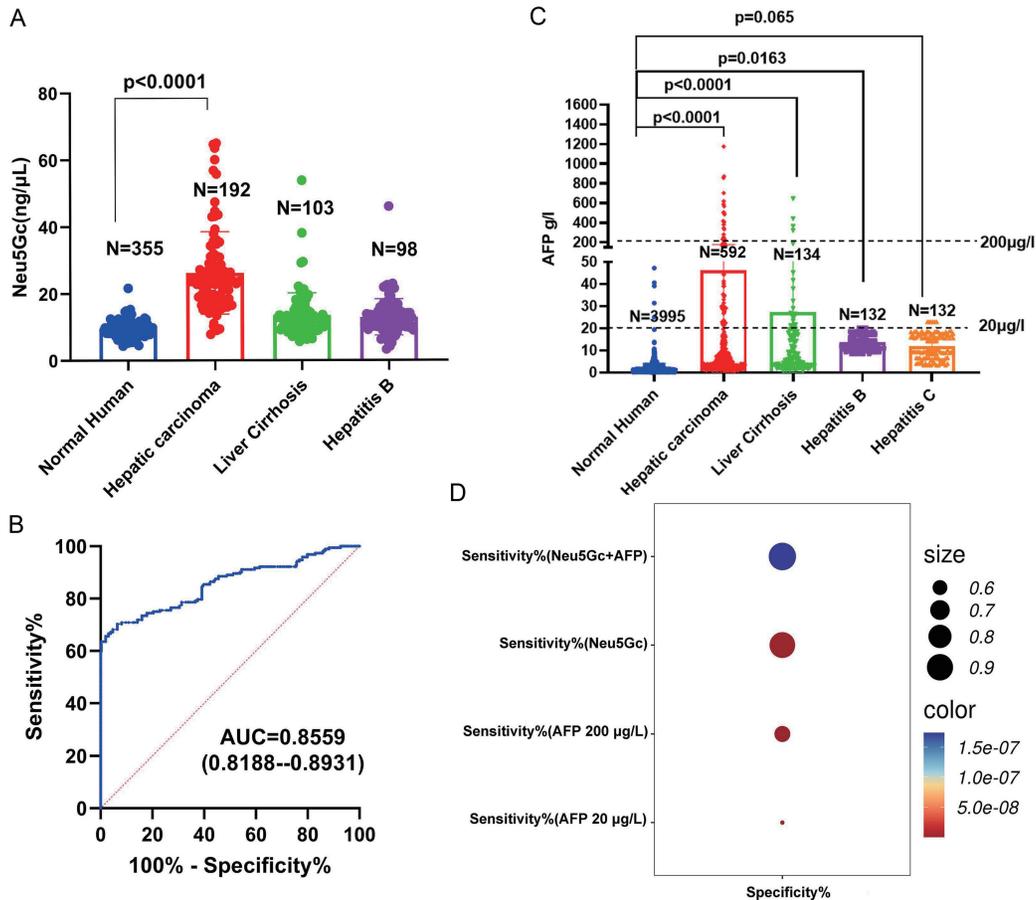
Fig. 2. Identification of Neu5Gc-modified target protein and evaluation of its combined application with AFP. (A) The prospective validation cohort was pre-coated with IgG antibody using the sandwich method, and the IgG glycoprotein in each group was detected by LIP-ELISA to recognize the sialylated N-glycan Neu5Gc terminal. (B) ROC curves of the LIP-positive sialylated N-glycan Neu5Gc terminal of IgG as a biomarker panel for different groups versus healthy participants. AUC values of 0.8559 (prospective cohort) and 0.919 (retrospective cohort) with corresponding 95% CI are presented. (C) Serum AFP levels in healthy subjects and patients with HCC, LC, and CHB in the retrospective validation cohort. (D) Bubble diagram showing the sensitivity (81.69%), specificity (96.02%), and diagnostic accuracy (94.64%) of Neu5Gc combined with AFP in parallel detection mode. ROC, receiver operating characteristic; Neu5Gc, N-glycolylneuraminic acid; LIP, lamprey immune protein; HCC, hepatocellular carcinoma; LC, liver cirrhosis; CHB, chronic hepatitis B; CHC, chronic hepatitis C; AUC, area under the curve; CI, confidence interval; AFP, alpha-fetoprotein.

Table 1. Statistics of double-index combined diagnosis of HCC

	Sensitivity%	Specificity%	AUC
AFP	36.11	96.3	0.6271
AFP (20 µg/L)	25	99.85	
AFP (400 µg/L)	3.28	100	
Neu5Gc	57.77	99.91	0.8441
Neu5Gc (22.85 ng/µL)	73.99	99.94	
Fucose	37.5	97.92	0.724
Fucose (0.6084 OD)	83.33	66.67	
Neu5Gc+AFP	81.93	99.94	
Neu5Gc+Fucose	91.67	66.67	

Parentheses indicate biomarker cutoff thresholds. Missing AUC values reflect analyses focused on optimal cutoffs rather than full ROC curve quantification. Combined markers represent dual-marker diagnostic strategies. AFP, alpha-fetoprotein; Neu5Gc, N-glycolylneuraminic acid; Fucose, L-fucose; AUC, area under the ROC curve; OD, optical density; ROC, receiver operating characteristic; HCC, hepatocellular carcinoma.

sites of the basic B/Y ions and the corresponding mass spectrum peaks matched the complete glycan structures. This analysis identified 13 characteristic glycan structures shared by healthy subjects and HCC patients, while two unique glycan chains were identified in healthy subjects and six were specific to the HCC group. Terminal Neu5Gc-modified glycan structures are illustrated in Figure 3C. The observed differences in glycan structures could be attributed to enhanced glycosylation, driven by an increased abundance of multi-branched glycan chains. We classified and compared 220 glycan chain structures based on variations in their terminal monosaccharides (Fig. 3D). For Neu5Gc-terminated glycan structures, notable changes included a 2.7-fold increase in afucosylated forms, a 3.3-fold increase in core-fucosylated forms, and a 2.9-fold increase in terminal-fucosylated forms. Additionally, glycan chain profiling was performed for structures terminated by other monosaccharides, including mannose, Neu5Ac, galactose, core fucose, sialyl Lewis A (SLeA), and sialyl Lewis X (SLeX). Serum IgG-derived Neu5Gc-terminated N-glycoproteins in HCC patients were significantly elevated, and levels of other monosaccharide-modified glycans were also substantially increased in the HCC group.
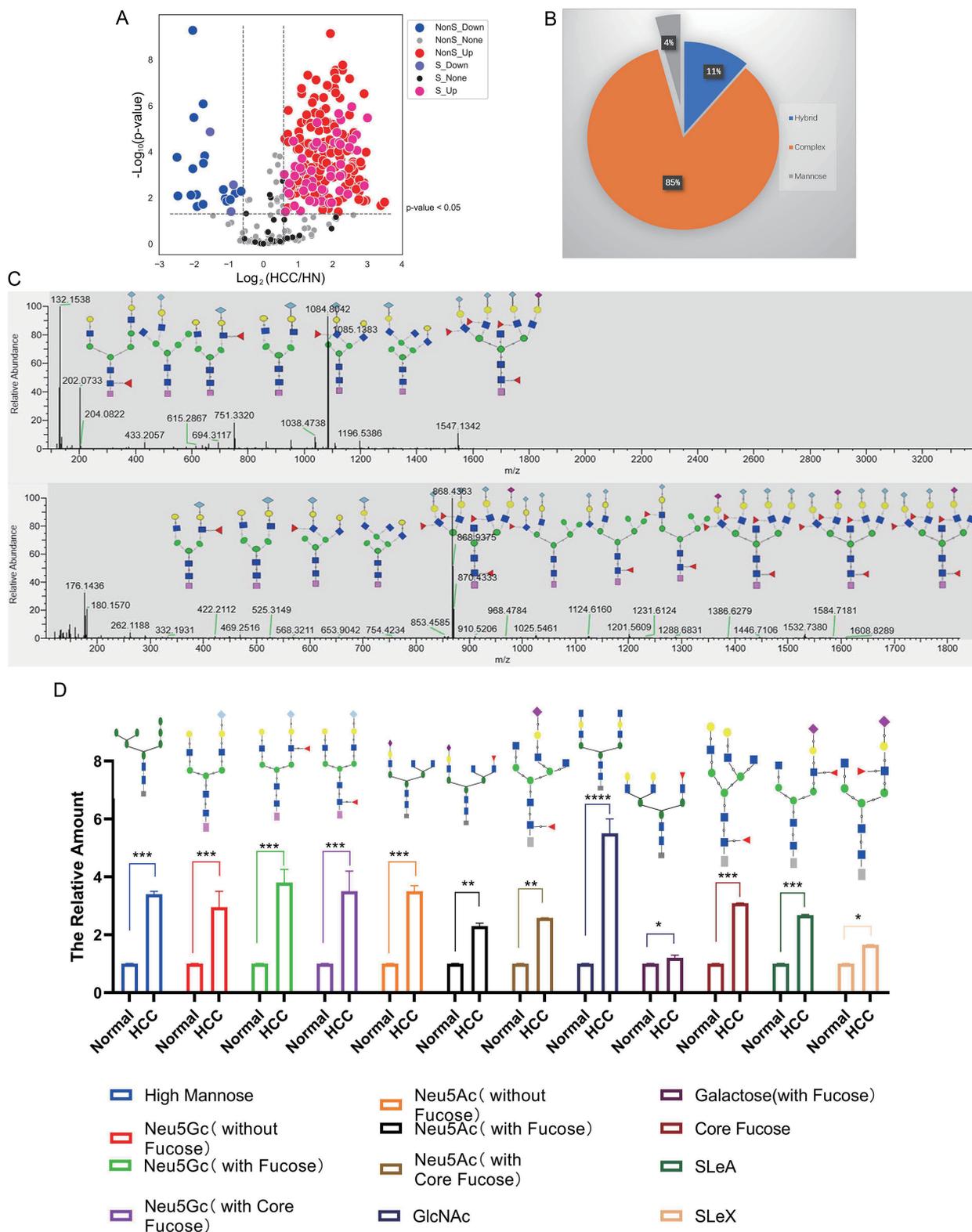
We further analyzed public databases for enzymes in-

Fig. 3. Isotopic labeling for quantitative identification of IgG by N-glycoproteomics. (A) Volcano plot of the final screened N-glycopeptides (fold change > 1.5, $P < 0.05$; n = 244). (B) Pie chart showing the proportional distribution of N-glycan types. (C) Termini of the healthy subjects and the HCC group corresponding to the B/Y-ion peak diagram containing N-glycopeptides modified by Neu5Gc. (D) Statistical comparisons of the modification levels of distinct terminal monosaccharide moieties between the HCC and healthy groups. The statistical analysis was performed using an unpaired two-sample *t*-test. Neu5Gc, N-glycolylneuraminic acid; HCC, hepatocellular carcinoma. *$P < 0.05$; **$P < 0.01$; ***$P < 0.001$; ****$P < 0.0001$.
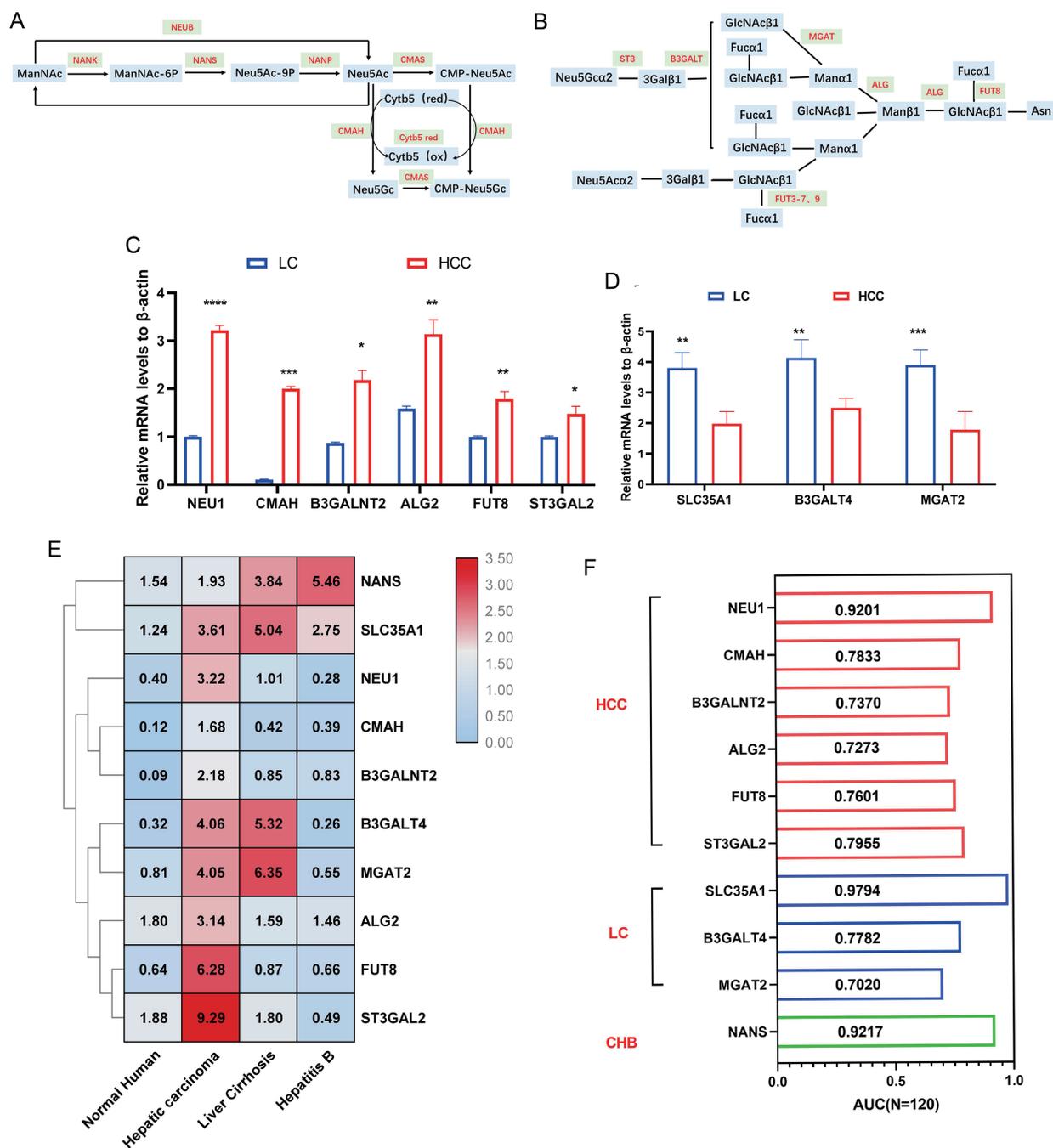
Fig. 4. Screening and validation of glycosylation-associated gene panels for multi-target differential diagnosis of HCC. (A–B) Biosynthetic pathway of Neu5Gc and canonical N-glycosylation modification pathway derived from the KEGG database. (C) qRT-PCR validation of genes significantly upregulated in the HCC group relative to the LC group (*NEU1, CMAH, B3GALNT2, ALG2, FUT8, ST3GAL2*). (D) qRT-PCR validation of gene expression predominantly expressed in the LC group (*SLC35A1, B3GALT4, MGAT2*) and the gene with the highest expression in the CHB group (*NANS*). (C–D, RNA was extracted from PBLs and reverse-transcribed into cDNA. Data are shown as histograms. Statistical analysis was performed using the Wilcoxon rank-sum test). (E) Heatmap of the 10 key differentially expressed glycosylation-related genes validated by qRT-PCR. Unsupervised clustering illustrates similarities in expression patterns across clinical groups. (F) Histogram showing AUC values with 95% CIs for the 10 candidate genes, calculated based on subgroup-specific high-expression signatures. Neu5Gc, N-glycolylneuraminic acid; HCC, hepatocellular carcinoma; LC, liver cirrhosis; CHB, chronic hepatitis B; AUC, area under the curve; CI, confidence interval; PBLs, peripheral blood leukocytes. $*P < 0.05$; $**P < 0.01$; $***P < 0.001$; $****P < 0.0001$.

volved in Neu5Gc biosynthesis (Fig. 4A) and glycan modification (Fig. 4B). Using data from The Cancer Genome Atlas and the UALCAN database (Supplementary Fig. 3D), 25 genes with significant expression changes were identified and subsequently validated by qRT-PCR using RNA extracted from peripheral blood leukocytes of clinical patients. qRT-PCR analysis demonstrated significantly higher expression levels of *NEU1, CMAH, B3GALNT2, ALG2, FUT8,* and *ST3GAL2* in

HCC than in the LC group (Fig. 4C), indicating their potential utility in the differential diagnosis of HCC. Conversely, *SLC35A1, B3GALT4,* and *MGAT2* were most highly expressed in the LC group (Fig. 4D), while *NANS* exhibited the highest expression in the CHB group relative to other groups.

These findings suggest that a combination of these differentially expressed genes could serve as effective diagnostic markers to distinguish HCC, LC, and CHB. To validate this, a heat map for the 10 key differentially expressed genes was generated (Fig. 4E), and AUC analysis was performed for each individual gene (Fig. 4F). The differential expression profiles of these genes across groups effectively distinguished HCC from other liver diseases. Further investigation using the Human Protein Atlas database (Supplementary Fig. 3E) revealed that the expression levels of the corresponding proteins in HCC tissues also exhibited an identical upregulation trend. Therefore, this study identified a panel of N-glycosylation-related genes that could serve as valuable markers for differential diagnosis of HCC.

Analysis of CMAH gene expression and mutations in HCC patients

The elevated levels of Neu5Gc in patients with HCC may suggest alterations in the enzyme responsible for the hydroxylation of Neu5Ac and its subsequent conversion to Neu5Gc *in vivo*. To investigate this, we analyzed the expression of *CMAH* in HCC patients. Western blotting (Fig. 5A and B) and immunohistochemistry (IHC) (Fig. 5C and D) demonstrated that CMAH protein expression was significantly upregulated in both diethylnitrosamine-induced HCC and human HCC tissues. Peritumoral non-tumor liver tissues, which often exhibited pronounced cirrhosis, also showed moderate positivity for CMAH. In contrast, tissues with normal liver morphology at the tumor margin were negative for CMAH. Notably, nearly all human HCC tissue sections displayed intense, diffuse CMAH immunostaining, indicating selective upregulation of CMAH in HCC tumor tissues relative to normal hepatic tissues.

To further characterize CMAH genetic alterations in HCC, nested PCR targeting the human CMAH locus was performed on gDNA and cDNA reverse-transcribed from RNA isolated from peripheral blood leukocytes of HCC patients. As shown in Figure 5E1, agarose gel electrophoresis confirmed the high quality of the extracted RNA and DNA, supporting the credibility of the experimental results. Two rounds of nested PCR were conducted, generating shorter cDNA-derived amplicons and longer gDNA-derived fragments (Fig. 5E2). The amplified DNA was excised from the gel, purified (Fig. 5E3), and concentrated (Fig. 5E4) for subsequent cloning. The purified target fragment was ligated into a T-vector for Sanger sequencing. The ligation product was transformed into *Escherichia coli* competent cells, which were plated on selective solid medium, and single colonies were picked for propagation. Colony PCR was performed to screen for positive clones with successful ligation (Fig. 5E5). Qualified single colonies were expanded, and plasmids were extracted after reaching logarithmic growth (Fig. 5E6). PCR amplification with T-vector primers yielded plasmid samples suitable for sequencing (Fig. 5E7). Sanger sequencing revealed multiple alterations in the amplified sequences from the HCC samples, including single nucleotide additions or deletions (Supplementary Fig. 4A). BLAST analysis against the NCBI database confirmed that the amplified gene was the human *CMAH* gene (Supplementary Fig. 4B). Conversion of the nucleotide sequence to an amino acid sequence using ORF Finder showed a high degree of sequence homology (Supplementary Fig. 4C), confirming that the amplified product contained a complete CDS region with a continuous coding sequence. Motif analy-

sis revealed substantial changes in the motif sequences of the HCC samples, including numerous gene mutations (Supplementary Fig. 4D). While motifs 1–5, which constitute the ULAG superfamily domain, were conserved in normal genomic sequences, post-sequencing results showed that only motif 1 remained conserved, while motifs 4–5 were replaced by motifs 6–9 (Supplementary Fig. 4E). This indicated significant alterations in the amino acid sequence of the HCC group, although the corresponding domain was still formed. Analysis of CMAH using the TSVdb gene splicing tool (Supplementary Fig. 4F) revealed multiple SNP mutations across various exons, which may contribute to aberrant transcription in tumors. According to the Ensembl database (Fig. 5F), which provides comprehensive genomic information, all detected mutations in *CMAH* were cataloged (Fig. 5G). The Ensembl platform supports studies on comparative genomics, sequence variation, transcriptional regulation, and gene annotation, providing a basis for understanding gene function and associated diseases. A diagram of the alternative splicing patterns of *CMAH* in HCC was constructed based on the sequencing results (Fig. 5H). Our experimental validation and data analysis suggest that *CMAH* may undergo mutations under tumor conditions, leading to a high likelihood of alternative splicing and potential gene reactivation. Additionally, the elevated expression of CMAH protein detected in the peripheral blood leukocytes and tissues of HCC patients indicates the presence of a CMAH-dependent Neu5Gc synthesis pathway in tumors, which is potentially detectable by LIP.

Enhancement of sialic acid synthesis in HCC cells via exogenous glycan intake in vitro

After successfully establishing a cellular hypoxia model using SMMC-7721 cells induced by $CoCl_2$, the cells were incubated with 30 mM Neu5Gc (end product), CMP-Neu5Ac (intermediate product), or UDP-GlcNAc (HBP pathway product and a substrate for polysaccharide synthesis) for 48 h. Glycan substrates were replenished every 12 h, and the treated cells were collected for high-content detection (Supplementary Fig. 5A). The levels of Neu5Gc on the cell surface were analyzed using flow cytometry (Supplementary Fig. 5B) and confocal imaging (Supplementary Fig. 5C) with LIP. After culturing with human serum for 10 days, Neu5Gc was barely detected on the cell surface. However, once hypoxia-inducible factor (HIF) expression stabilized, exogenous glycan substrates (30 mM) were added to supplement glycosylation precursors. After 48 h, the levels of Neu5Gc were restored or exceeded the basal levels typically found in tumor cells. It was observed that the Neu5Gc content in the cell membrane significantly increased, particularly in hypoxia-treated cells. Additionally, metabolomic analysis was performed on samples collected at various time points (0, 1, 12, 24, 36, and 48 h), identifying a total of 2,966 metabolites, including differentially expressed metabolites (Supplementary Fig. 5D and E).

To elucidate the regulatory mechanism of sialic acid synthesis in HCC cells, we focused on tracking the levels of key intermediates at different time points to infer their metabolic sequence. Temporal changes in intermediate metabolites along the sialic acid synthesis pathway over time were observed (Fig. 6A and Supplementary Fig. 5F). This non-targeted metabolomics approach effectively uncovered the metabolic pathways involved. As shown in Figure 6B, isotope labels were detected for three metabolites, including glucose-6-phosphate, which is involved in glycolysis and gluconeogenesis. Additionally, five intermediate metabolites in the tricarboxylic acid cycle, acetyl-CoA, and malic acid were identified. Amino acid metabolism provided the carboxyl groups essential for sialic acid synthesis. The two metabolic
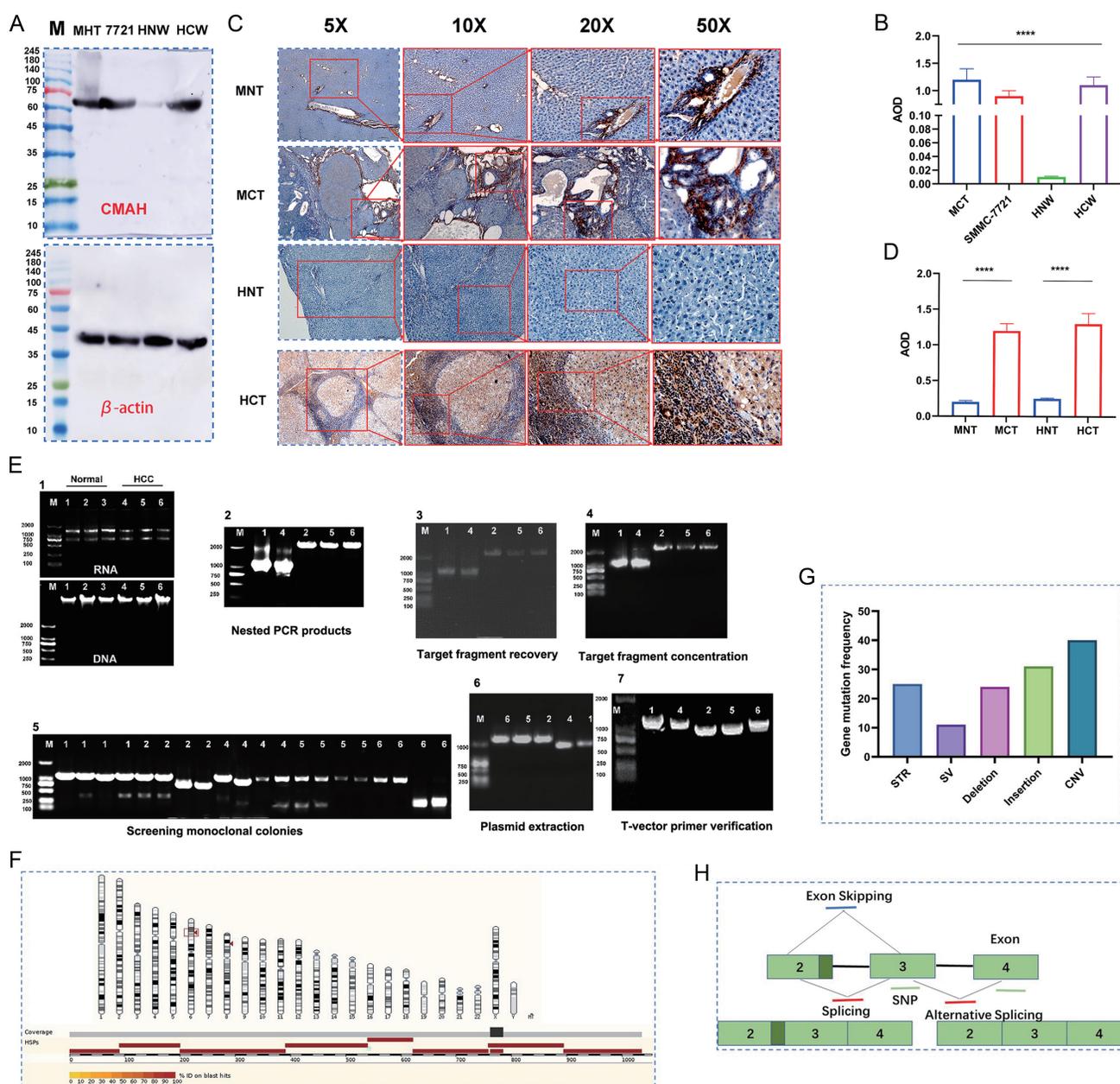
Fig. 5. CMAH expression in HCC and sequence analysis of the *CMAH* gene. (A) Expression of CMAH protein in MCT, liver cancer cell line SMMC-7721 (7721), HNW, and white blood cells from patients with HCC (HCW) detected by Western blotting. (B) Quantitative statistical analysis of WB band densities in A, calculated as AOD using ImageJ software. (C) Expression of CMAH protein in mouse HCC tissue, MNT, MCT, HNT, and HCT detected by IHC. (D) Quantitative statistical analysis of IHC intensity in C, quantified as AOD using Image-Pro Plus 6.0 software. (E) 1. Amplification and sequencing of *CMAH* gene sequence: RNA extraction and genomic DNA extraction results; 2. Nested PCR amplification results; 3. Recovered target segment; 4. Concentrated recovered target fragment; 5. PCR test results of monoclonal colony after ligation and transformation; 6. Plasmid extraction after T-vector insertion; 7. Vector primer PCR verification. (F) Overview of CMAH genetic variations in the chr6:25080000–25130000 locus. (G) Aberrant alternative splicing patterns of *CMAH* in HCC. (H) Diagram of alternative splicing events. Data are presented as means ± S.D.; n = 45 biological replicates per group. HCC, hepatocellular carcinoma; AOD, average optical density; IHC, immunohistochemistry; PCR, polymerase chain reaction; MCT, mouse HCC tissue; HNW, normal white blood cells; MNT, normal liver tissues of mice; HNT, human paracancerous tissue; HCT, human HCC tissue. *$P < 0.05$; **$P < 0.01$; ***$P < 0.001$; ****$P < 0.0001$.

pathways most directly linked to sialic acid synthesis were the hexosamine biosynthetic pathway (HBP) and polysaccharide synthesis pathway.

To validate the proposed sialic acid synthesis pathway inferred from the metabolomics data, we determined the main pathways based on intermediate metabolites and screened for key target inhibitors. N-acetyl-2,3-dehydro-2-deoxyneu-

raminic acid is an effective neuraminidase inhibitor. Acriflavine hydrochloride, a preservative with antitumor activity, effectively inhibits HIF-1.[59] WB 117, an inhibitor of glucose transporter 1 (Glut 1), downregulates glycolysis, induces cell cycle arrest, and inhibits cancer cell growth both *in vitro* and *in vivo*.[60] Tanifluoric acid, a precursor of nifluoric acid, is converted by esterases *in vivo* to reduce the synthesis
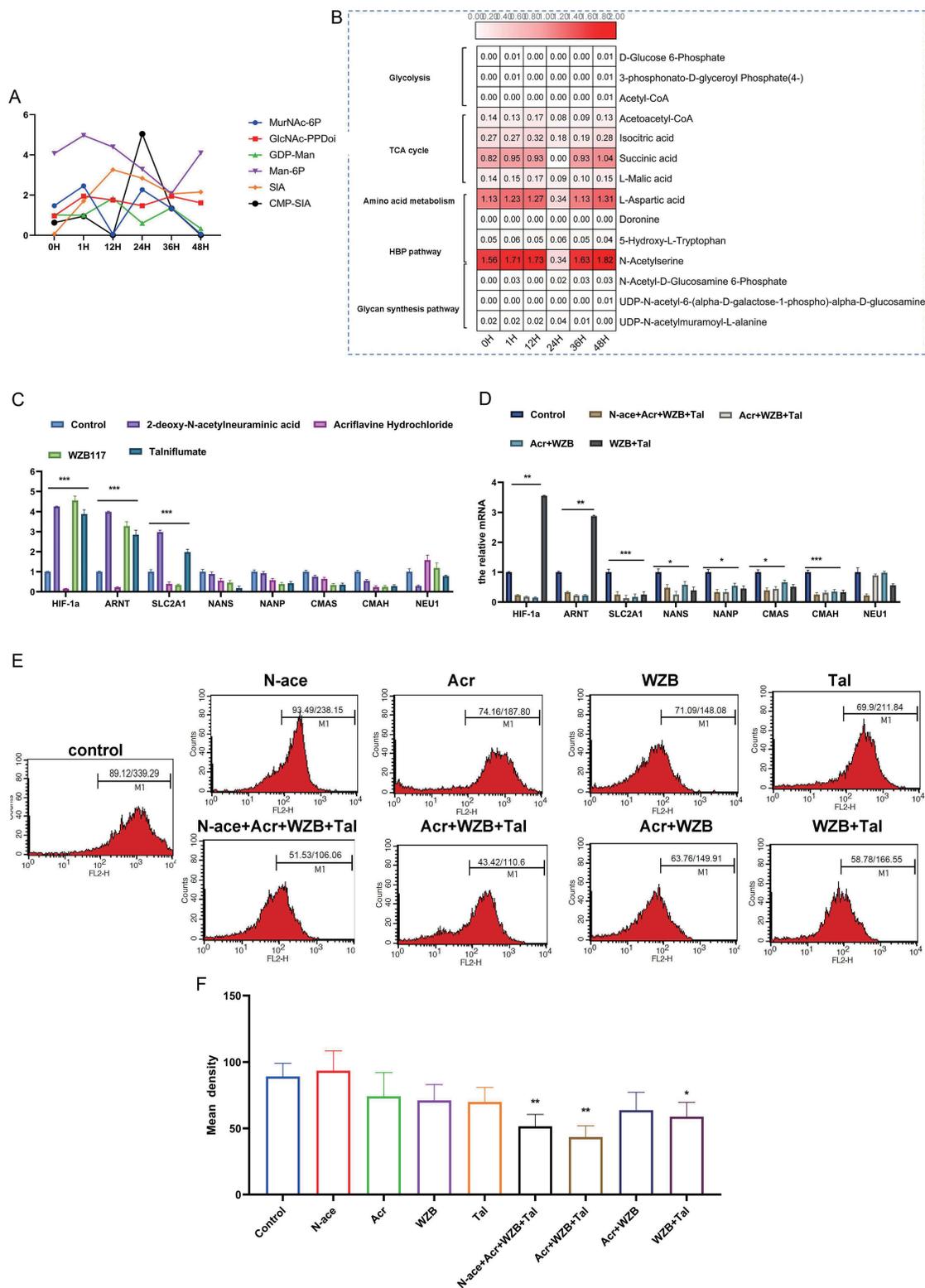
Fig. 6. Statistics of sialic acid intermediate metabolites based on time-series non-targeted metabolomics. (A) Changes in intermediate metabolites associated with sialic acid production, expressed as a scatter plot with bar (Wilcoxon rank-sum test). (B) Heatmap of intermediate metabolites in the time series. (C) Detection of hepatocellular carcinoma cells (SMMC-7721) treated with a single inhibitor by qRT-PCR. (D) qRT-PCR detection of SMMC-7721 under the action of combined inhibitors. (E) Flow cytometry detection of Neu5Gc content on the surface of hepatocellular carcinoma cells after inhibitor treatment. (F) Quantitative analysis of cell surface Neu5Gc levels from flow cytometry results in E. Data are presented as means ± S.D. (n = 3 biological replicates per group). Neu5Gc, N-glycolylneuraminic acid; PCR, polymerase chain reaction. *P < 0.05; **P < 0.01; ***P < 0.001; ****P < 0.0001.

and release of mucin in animal models and cell cultures.[61] The expression of genes related to the HIF pathway (HIF-1, ARNT/HIF-1β), glucose transport (SLC2A1/Glut 1), and sialic acid metabolism (NANS, NANP, MAS, CMAH, and NEU1) was assessed by qRT-PCR (Fig. 6C). The results of inhibitor experiments showed that each inhibitor effectively targeted the primary pathway. Acriflavine, an upstream pathway inhibitor, also inhibits downstream targets such as Glut 1 and sialic acid-related synthetases.[62] To verify the synergistic effects of these inhibitors, various combinations were tested to inhibit multiple pathways. As shown in Figure 6D, pairwise combinations excluding sialidase inhibitors were evaluated because sialidase inhibition alone did not affect sialic acid synthesis. The combined use of inhibitors confirmed their synergistic effects on the relevant pathways. Upregulation of the hypoxia and glucose transport pathways enhanced sialic acid synthesis, whereas sialic acid degradation downregulated its synthesis. Flow cytometry was subsequently used to measure the Neu5Gc content on the cell surface. As shown in Figures 6E and F, DANA alone effectively inhibited sialic acid degradation. The results obtained with other inhibitors, whether used alone or in combination, were largely consistent with the qRT-PCR results (Fig. 6C and D).

As illustrated in Supplementary Figures 5G and H, KEGG enrichment analysis demonstrated that the differential metabolites were mainly involved in amino acid metabolism and linked energy/carbohydrate metabolic pathways, with concomitant alterations in lipid, vitamin, and transport-related biological processes. Metabolite expression statistics at different time points revealed increased consumption of glucose-6-phosphate and 3-phospho-D-glycerophosphate during glycolysis and gluconeogenesis. In addition, the consumption of aspartic acid and N-acetylserine, which are related to succinic acid and amino acid metabolism, peaked at 24 h in the tricarboxylic acid cycle before output increased, leading to the synthesis of sialic acid in cells. This synthesis is associated with the HBP and polysaccharide synthesis pathway.

Effect of an exogenous high-sialic acid diet on Neu5Gc content in peripheral blood and liver tissue in vivo

Bioinformatic database analysis highlighted the critical role of the *CMAH* gene in its activated state, as it promotes the hydroxylation of Neu5Ac to Neu5Gc. To investigate this further, a *CMAH* gene knockout mouse model ($CMAH^{-/-}$) was constructed (Supplementary Fig. 6A–D), wherein sialic acid metabolism resembled that of normal human metabolism. In the absence of the *CMAH* gene, Neu5Gc in humans comes exclusively from exogenous absorption and ingestion. In the experimental model, commercial Neu5Ac monosaccharide and mucin (extracted from porcine submandibular glands) were added to the diet at a concentration of 100 µg/g. As shown in Figure 7A, serum Neu5Gc levels in $CMAH^{-/-}$ mice increased progressively with the intake of an exogenous diet, eventually reaching levels comparable to those in wild-type mice. This indicates that endogenous synthesis of Neu5Gc can be fully compensated for by an exogenous source, maintaining Neu5Gc levels in the animal (Fig. 7B).

Time-series analysis and metabolomic data demonstrated that sialic acid synthesis is influenced by both exogenous intake and endogenous production. As shown in Figure 7C, mice fed a high-fat diet (HFD) exhibited a significant increase in blood lipid levels and Neu5Gc content. This prompted further examination of changes in the hypoxia pathway in mice stimulated by an exogenous diet, as depicted in Figure 7D

and E. IHC for HIF-1α, GLUT1, VEGF, CMAH, LIP, and SNA lectin revealed that fatty lesions developed in the liver tissue of mice subjected to both HFD and HFD supplemented with sialic acid. In *CMAH* knockout mice, exogenous feeding upregulated HIF-1α expression, which was primarily localized in hepatocytes. Additionally, it increased the expression of GLUT1, enhancing glucose utilization without clear tissue specificity. VEGF expression was also upregulated, especially in regions with increased angiogenesis and fibroblasts. However, as expected, CMAH protein expression was barely detectable in the liver tissues of $CMAH^{-/-}$ mice, confirming the success of the knockout model.

When the HFD was combined with high sialic acid, there was a significant increase in the detection of LIP and SNA, indicating a synergistic crosstalk between the hypoxia pathway and sialic acid synthesis pathway, rather than mere corroboration. Collectively, these findings demonstrate that both exogenous dietary sialic acid intake and altered endogenous synthesis can modulate cellular metabolic pathways, forming a feedback loop that regulates Neu5Gc accumulation (Fig. 7F).

Discussion

In this study, a comprehensive platform for detecting blood Neu5Gc levels was established for diagnosing HCC, and the possible mechanisms underlying elevated Neu5Gc levels were evaluated. We also explored the changes in glycan-related genes during Neu5Gc anabolism and glycosylation, shedding light on the endogenous Neu5Gc synthesis pathway. Prior studies indicate that exogenous Neu5Gc, primarily from dietary red meat and dairy, is incorporated into cell-surface glycans and preferentially accumulates in cancer cells.[63] Notably, the tumor-specific antigen GM3 (Neu5Gc) is present in various human cancers.[64] Also, Neu5Gc promotes CRC cell proliferation through Wnt/β-catenin activation.[65] This validates its oncogenic significance and potential as a pan-tumor biomarker for HCC and other malignancies. Additionally, we observed that Sprague–Dawley rats possess the *CMAH* gene with slight variations compared to humans. However, analysis of the expression of the human *CMAH* gene revealed its research value, warranting further investigation into its *in vivo* regulation. Humans carry a non-functional CMAH pseudogene due to an ancient Alu-mediated deletion,[9–10] and human Neu5Gc is primarily derived from exogenous dietary sources such as red meat,[66,67] providing a critical evolutionary context for our mechanistic exploration.

To simulate the human environment, we constructed a *CMAH* knockout mouse using the CRISPR-Cas9 platform. This allowed us to explore the compensatory mechanism of exogenous intake following the inactivation of the endogenous synthesis pathway. *CMAH*-deficient mouse models have been used to study Duchenne muscular dystrophy,[68,69] metabolic disorders,[70] atherosclerosis,[11] and cancers[71]; our application to Neu5Gc metabolism and tumor immunology is a key innovation. We then employed isotope-labeled glycosaminoglycan substrates and tracked isotope incorporation at different time points to construct a non-targeted isotope-labeled metabolic pathway. This approach revealed potential metabolic routes for sialic acid substrates in cells, offering insights into the possible mechanisms of abnormally high Neu5Gc levels in HCC. Isotope tracing has been widely applied to map sialic acid metabolic fluxes in cancer cells, enabling unbiased identification of key pathway intermediates.[72–74] Key findings in metabolomics were validated by feeding hepatic cancer tissue a high-sialic acid diet. We conducted experiments using gene knockout mice and added exogenous glycine to HCC
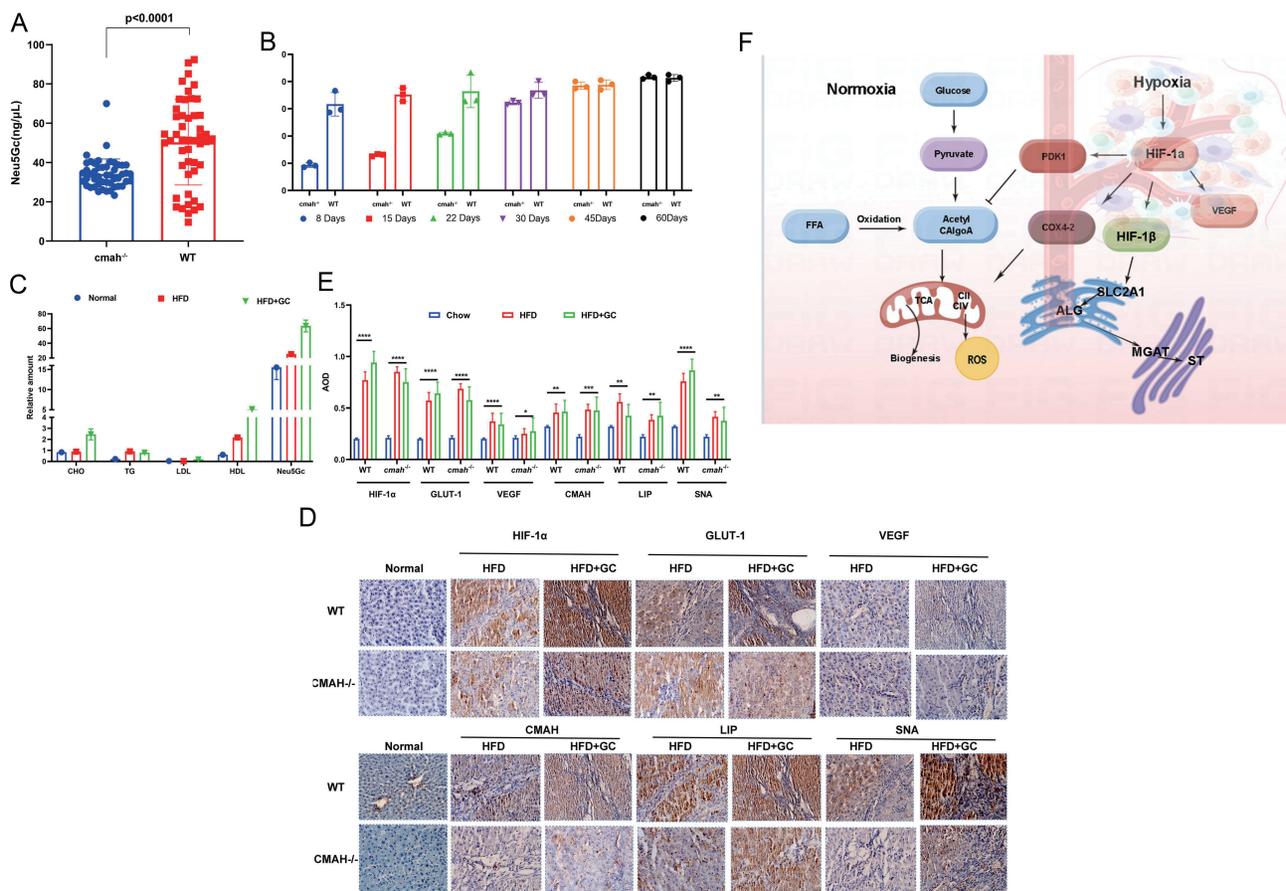
Fig. 7. Effect of an exogenous high-sialic acid diet on Neu5Gc content in peripheral blood and liver tissue of *CMAH*$^{-/-}$ mice. (A) Comparison of serum Neu5Gc content between WT mice and *CMAH*$^{-/-}$ mice. Data are expressed as a scatter plot with bar (unpaired two-sample *t*-test). (B) Comparison of serum Neu5Gc content between WT mice and *CMAH*$^{-/-}$ mice after long-term high sialic acid diet feeding. (C) Changes in serum indicators in mice fed with high sialic acid. (D) Quantitative analysis of IHC results, presented as AOD. (E) IHC detection of the influence of an exogenous high-sialic acid diet on Neu5Gc in mice. (F) Proposed mechanism of tumor-induced abnormal increase of Neu5Gc. Data are shown as means ± S.D. (for cell experiments, n = 3 biological replicates per group, consistent with the experimental design of previous sections). Neu5Gc, N-glycolylneuraminic acid; AOD, average optical density; IHC, immunohistochemistry; HFD, high-fat diet. *$P <$ 0.05; **$P <$ 0.01; ***$P <$ 0.001; ****$P <$ 0.0001.

cell lines to explore the mechanisms responsible for the high Neu5Gc levels on the surface of tumor cells. This revealed endogenous self-synthesis via the HBP hexosamine pathway. In this pathway, the intermediate metabolite UDP-GlcNAc is isomerized by epimerase, leading to sialic acid production. As a central hub linking glucose metabolism to protein glycosylation, the HBP modulates glycosylation via its rate-limiting enzymes and metabolites, facilitating HCC proliferation and metastasis.[75–77] Notably, there may be CMAH proteins or CMAH protein subtypes in tumor cells that perform certain hydroxylation functions.[78] Recent studies suggest that CMAH pseudogene-derived transcripts or truncated proteins may retain partial biological activity in certain cancers, possibly including HCC,[79,80] which aligns with our observation of potential residual CMAH function.

However, no additional information is currently available regarding this pathway, necessitating further research. Generally, there are two main reasons for the high surface levels of Neu5Gc in tumor cells: endogenous synthesis and exogenous intake. The endogenous synthesis pathway includes reactivation of the CMAH-dependent pathway and compensation of the non-CMAH-dependent pathway. Nevertheless, exogenous intake is still dominant, which may depend on many factors, such as excessive intake of red meat caused by regional and individual differences in eating habits. Exogenous Neu5Gc enters cells via pinocytosis, enhanced in tumors by macropinocytosis and altered transporters.[71] Hypoxia caused by the rapid proliferation of tumor cells significantly increases intracellular glucose metabolism. Because of the high metabolic characteristics of tumor cells, the uptake ability of exogenous glycosylated glycan substrates is stronger than that of normal cells, and Neu5Gc is highly expressed in different patients. Hypoxia further promotes Neu5Gc accumulation by upregulating sialyltransferases and enhancing exogenous glycan uptake.[81,82]

According to the theory of "aerobic glycolysis" in tumor cell metabolism, reprogramming of glucose metabolism is driven by continuous activation of oncogenes or inactivation of tumor suppressor genes.[83] The hypoxic microenvironment plays a crucial role in cancer development and therapeutic response, leading to continuous interactions between cancer cells and stromal cells. The Warburg effect and tumor hypoxia collectively drive metabolic reprogramming that favors sialic acid synthesis and exogenous Neu5Gc uptake.[84] In this study, we observed an increase in Neu5Gc accumulation on the tumor cell surface under hypoxic conditions, shedding light on the degree of glycosylation and its potential mechanisms. Our findings extend previous reports by linking hy-

poxia-induced metabolic reprogramming to aberrant Neu5Gc glycosylation in HCC, highlighting a novel regulatory axis.

However, as a pioneering effort, our study has certain limitations in terms of the experimental design and detection technology. In this study, glycan analysis was performed on a single protein in the serum. Although IgG is a highly abundant protein, it cannot fully represent the glycosylation profile of the total serum proteins. Additionally, the follow-up cohort in this study was a dynamic cohort with a duration of more than 10 years. However, this was presented in a cross-sectional manner in this study, failing to reflect the dynamic advantages of the cohort. Further stratified analysis was not performed to establish a clinical prediction model. Additionally, the mechanistic research was not sufficiently deep, and the integration of mouse and cell experiments was insufficient. The evidence presented here lacks direct intuitiveness, emphasizing the need for further validation of this pathway. To address this, we aimed to establish a metabolic flow detection platform focusing on sialic acids Neu5Ac and Neu5Gc to enhance the clarity of our findings. Future studies will integrate multi-omics data and longitudinal cohort analysis to develop a clinically applicable Neu5Gc-based diagnostic model for HCC, addressing current limitations and translating our findings into clinical practice.

Conclusions

Neu5Gc represents a promising biomarker for HCC diagnosis and therapy evaluation. Our dual strategy improves diagnostic sensitivity, and an N-glycosylation-related gene panel was identified for HCC differential diagnosis. Mechanistically, CMAH mutations induce alternative splicing and Neu5Gc synthesis, while metabolic reprogramming promotes sialic acid production. Together, exogenous Neu5Gc intake and endogenous metabolic changes form a feedback loop that promotes HCC progression. These results offer new insights for the development of diagnostic biomarkers and therapeutic targets in HCC.

Conflict of interest

The authors have no conflict of interests related to this publication.

Author contributions

Experimental testing (XC), data curation (XC, XL, XS, CP), original draft preparation (XC), software (XC, JL), visualization (XC, JL), investigation (XC), sample collection (XL, XS, CP), conceptualization (QL, YP), methodology (QL, YP), validation (QL, YP), supervision (YH), and writing–reviewing and editing (YP). All authors have approved the final version and publication of the manuscript.

Ethical statement

This study was approved by the Ethics Committees of Dalian Public Health Clinical Center (No. 2021-016-002), Affiliated Zhongshan Hospital of Dalian University (No. 2021053-1), and Liaoning Normal University (No. LL2020015) and was conducted from January 2020 to June 2022 in accordance with the Declaration of Helsinki (as revised in 2024). All participants provided written informed consent.

Data sharing statement

All data used and analyzed in this study are included in the main text of this article and the supplementary information files. For other unprocessed raw data and patient-related de-identified information, those in need can contact the first author or corresponding author.

References

[1] Samant H, Amiri HS, Zibari GB. Addressing the worldwide hepatocellular carcinoma: epidemiology, prevention and management. J Gastrointest Oncol 2021;12(Suppl 2):S361–S373. doi:10.21037/jgo.2020.02.08, PMID:34422400.

[2] Ji D, Chen Y, Bi J, Shang Q, Liu H, Wang JB, *et al*. Entecavir plus Biejia-Ruangan compound reduces the risk of hepatocellular carcinoma in Chinese patients with chronic hepatitis B. J Hepatol 2022;77(6):1515–1524. doi:10.1016/j.jhep.2022.07.018, PMID:35985545.

[3] Lin H, Lee HW, Yip TC, Tsochatzis E, Petta S, Bugianesi E, *et al*. Vibration-Controlled Transient Elastography Scores to Predict Liver-Related Events in Steatotic Liver Disease. JAMA 2024;331(15):1287–1297. doi:10.1001/jama.2024.1447, PMID:38512249.

[4] Dalbeni A, Lombardi R, Henrique M, Zoncapè M, Pennisi G, Petta S, *et al*. Diagnostic accuracy of AGILE 3+ score for advanced fibrosis in patients with NAFLD: A systematic review and meta-analysis. Hepatology 2024;79(5):1107–1116. doi:10.1097/HEP.0000000000000694, PMID:37976417.

[5] Ogawa K, Kobayashi T, Furukawa JI, Hanamatsu H, Nakamura A, Suzuki K, *et al*. Tri-antennary tri-sialylated mono-fucosylated glycan of alpha-1 antitrypsin as a non-invasive biomarker for non-alcoholic steatohepatitis: a novel glycobiomarker for non-alcoholic steatohepatitis. Sci Rep 2020;10(1):321. doi:10.1038/s41598-019-56947-1, PMID:31941930.

[6] Zhao Q, Zhan T, Deng Z, Li Q, Liu Y, Yang S, *et al*. Glycan analysis of colorectal cancer samples reveals stage-dependent changes in CEA glycosylation patterns. Clin Proteomics 2018;15:9. doi:10.1186/s12014-018-9182-4, PMID:29507546.

[7] Youssef FS, Ashour ML, El-Beshbishy HA, Singab ANB, Wink M. Metabolic Profiling of Buddleia indica Leaves using LC/MS and Evidence of their Antioxidant and Hepatoprotective Activity Using Different In Vitro and In Vivo Experimental Models. Antioxidants (Basel) 2019;8(9):412. doi:10.3390/antiox8090412, PMID:31540477.

[8] Singal AG, Haaland B, Parikh ND, Ozbay AB, Kirshner C, Chakankar S, *et al*. Comparison of a multitarget blood test to ultrasound and alpha-fetoprotein for hepatocellular carcinoma surveillance: Results of a network meta-analysis. Hepatol Commun 2022;6(10):2925–2936. doi:10.1002/hep4.2045, PMID:35945907.

[9] Dhar C, Sasmal A, Varki A. From "Serum Sickness" to "Xenosialitis": Past, Present, and Future Significance of the Non-human Sialic Acid Neu5Gc. Front Immunol 2019;10:807. doi:10.3389/fimmu.2019.00807, PMID:31057542.

[10] Okerblom J, Varki A. Biochemical, Cellular, Physiological, and Pathological Consequences of Human Loss of N-Glycolylneuraminic Acid. Chembiochem 2017;18(13):1155–1171. doi:10.1002/cbic.201700077, PMID:28423240.

[11] Kawanishi K, Dhar C, Do R, Varki N, Gordts PLSM, Varki A. Human species-specific loss of CMP-N-acetylneuraminic acid hydroxylase enhances atherosclerosis via intrinsic and extrinsic mechanisms. Proc Natl Acad Sci U S A 2019;116(32):16036–16045. doi:10.1073/pnas.1902902116, PMID:31332008.

[12] Saha S, Khan N, Comi T, Verhagen A, Sasmal A, Diaz S, *et al*. Evolution of Human-Specific Alleles Protecting Cognitive Function of Grandmothers. Mol Biol Evol 2022;39(8):msac151. doi:10.1093/molbev/msac151, PMID:35809046.

[13] Kooner AS, Yu H, Chen X. Synthesis of N-Glycolylneuraminic Acid (Neu5Gc) and Its Glycosides. Front Immunol 2019;10:2004. doi:10.3389/

fimmu.2019.02004, PMID:31555264.

[14] Blanco R, Muñoz JP. The Role of Non-Human Sialic Acid Neu5Gc-Containing Glycoconjugates in Human Tumors: A Review of Clinical and Experimental Evidence. Biomolecules 2025;15(2):253. doi:10.3390/biom15020253, PMID:40001556.

[15] Wang J, Shewell LK, Day CJ, Jennings MP. N-glycolylneuraminic acid as a carbohydrate cancer biomarker. Transl Oncol 2023;31:101643. doi:10.1016/j.tranon.2023.101643, PMID:36805917.

[16] Contò M, Miarelli M, Di Giovanni S, Failla S. Variability of Sialic Acids in Beef Breeds and Nutritional Implications in Red Meat. Molecules 2025;30(3):710. doi:10.3390/molecules30030710, PMID:39942813.

[17] Pang Y, Li C, Wang S, Ba W, Yu T, Pei G, *et al*. A novel protein derived from lamprey supraneural body tissue with efficient cytocidal actions against tumor cells. Cell Commun Signal 2017;15(1):42. doi:10.1186/s12964-017-0198-6, PMID:29037260.

[18] Pang Y, Gou M, Yang K, Lu J, Han Y, Teng H, *et al*. Crystal structure of a cytocidal protein from lamprey and its mechanism of action in the selective killing of cancer cells. Cell Commun Signal 2019;17(1):54. doi:10.1186/s12964-019-0358-y, PMID:31133022.

[19] Cao X, Yu S, Wang W, Sun R, Wu Z, Gao Z, *et al*. Lamprey immunity protein enables detection for bladder cancer through recognizing N-hydroxyacetylneuraminic acid (Neu5Gc)-modified as a diagnostic marker and exploration of its production mechanism. Biochem Biophys Res Commun 2022;614:153–160. doi:10.1016/j.bbrc.2022.04.121, PMID:35597152.

[20] Song X, Xu X, Lu J, Chi X, Pang Y, Li Q. Lamprey Immune Protein Mediates Apoptosis of Lung Cancer Cells Via the Endoplasmic Reticulum Stress Signaling Pathway. Front Oncol 2021;11:663600. doi:10.3389/fonc.2021.663600, PMID:34307136.

[21] Teng H, Li Q, Gou M, Liu G, Cao X, Lu J, *et al*. Lamprey immunity protein enables early detection and recurrence monitoring for bladder cancer through recognizing Neu5Gc-modified uromodulin glycoprotein in urine. Biochim Biophys Acta Mol Basis Dis 2022;1868(12):166493. doi:10.1016/j.bbadis.2022.166493, PMID:35853560.

[22] World Medical Association. World Medical Association Declaration of Helsinki: ethical principles for medical research involving human subjects. JAMA 2013;310(20):2191–2194. doi:10.1001/jama.2013.281053, PMID:24141714.

[23] Wong GL. Updated Guidelines for the Prevention and Management of Chronic Hepatitis B-World Health Organization 2024 Compared With China 2022 HBV Guidelines. J Viral Hepat 2024;31(Suppl 2):13–22. doi:10.1111/jvh.14032, PMID:39503252.

[24] Chinese Society of Gastroenterology, Chinese Medical Association. Chinese consensus on the management of liver cirrhosis. J Dig Dis 2024;25(6):332–352. doi:10.1111/1751-2980.13294, PMID:39044465.

[25] European Association for the Study of the Liver. EASL Clinical Practice Guidelines on the management of hepatocellular carcinoma. J Hepatol 2025;82(2):315–374. doi:10.1016/j.jhep.2024.08.028, PMID:39690085.

[26] Rafferty B, Mower JA, Ward HL, Rose M. Differences in carbohydrate composition of FSH preparations detected with lectin-ELISA systems. J Endocrinol 1995;145(3):527–533. doi:10.1677/joe.0.1450527, PMID:7636437.

[27] Ito H, Hoshi K, Honda T, Hashimoto Y. Lectin-Based Assay for Glycoform-Specific Detection of α2,6-sialylated Transferrin and Carcinoembryonic Antigen in Tissue and Body Fluid. Molecules 2018;23(6):1314. doi:10.3390/molecules23061314, PMID:29849005.

[28] Sato T. Lectin-probed western blot analysis. Methods Mol Biol 2014;1200:93–100. doi:10.1007/978-1-4939-1292-6_8, PMID:25117227.

[29] Phoomak C, Saengboonmee C, Baro M, Piriyapairoje K, Ittiudomrak T, Contessa JN, *et al*. High glucose enhances lung cancer cell aggressiveness: the impacts of GLUT1, UAP1, UGP2, and N-linked glycosylation. Glycobiology 2025;36(2):cwaf089. doi:10.1093/glycob/cwaf089, PMID:41452006.

[30] Wang Y, Isaji T, Wu T, Ono T, Saito T, Kuroda Y, *et al*. Hyaluronic acid regulates cellular UDP-GlcNAc levels through CD44 to affect glycosylation and cell biological functions. J Biol Chem 2026;302(2):111111. doi:10.1016/j.jbc.2025.111111, PMID:41461315.

[31] Li B, Gou M, Han J, Yuan X, Li Y, Li T, *et al*. Proteomic analysis of buccal gland secretion from fasting and feeding lampreys (Lampetra morii). Proteome Sci 2018;16:9. doi:10.1186/s12953-018-0137-5, PMID:29796011.

[32] Katayama H, Nagasu T, Oda Y. Improvement of in-gel digestion protocol for peptide mass fingerprinting by matrix-assisted laser desorption/ionization time-of-flight mass spectrometry. Rapid Commun Mass Spectrom 2001;15(16):1416–1421. doi:10.1002/rcm.379, PMID:11507753.

[33] Zheng R, Matzinger M, Mayer RL, Valenta A, Sun X, Mechtler K. A High-Sensitivity Low-Nanoflow LC-MS Configuration for High-Throughput Sample-Limited Proteomics. Anal Chem 2023;95(51):18673–18678. doi:10.1021/acs.analchem.3c03058, PMID:38088903.

[34] Wang Y, Xiao K, Tian Z. Quantitative N-glycoproteomics using stable isotopic diethyl labeling. Talanta 2020;219:121359. doi:10.1016/j.talanta.2020.121359, PMID:32887082.

[35] Pitarch A, Arribas V, Gil C. Omics and Multiomics-Based Diagnostics for Invasive Candidiasis: Toward Precision Medicine. Mol Cell Proteomics 2025;24(12):101463. doi:10.1016/j.mcpro.2025.101463, PMID:41237902.

[36] Li Y, Wang J, Chen W, Lu H, Zhang Y. Comprehensive review of MS-based studies on N-glycoproteome and N-glycome of extracellular vesicles. Proteomics 2024;24(11):e2300065. doi:10.1002/pmic.202300065, PMID:37474487.

[37] Luo H, Zhang Y, Yao Y, Zhang Q, Lin S, Wang S, *et al*. A novel galactoglucan from Ganoderma lucidum ameliorates ethanol-induced gastric ulcers by modulating FAK-MAPK signaling pathway. Carbohydr Polym 2025;360:123594. doi:10.1016/j.carbpol.2025.123594, PMID:40399003.

[38] Sule R, Rivera G, Gomes AV. Western blotting (immunoblotting): history, theory, uses, protocol and problems. Biotechniques 2023;75(3):99–114.

[39] doi:10.2144/btn-2022-0034, PMID:36971113.

[39] Takahashi Y, Dungubat E, Kusano H, Ganbat D, Tomita Y, Odgerel S, *et al*. Application of Immunohistochemistry in the Pathological Diagnosis of Liver Tumors. Int J Mol Sci 2021;22(11):5780. doi:10.3390/ijms22115780, PMID:34071338.

[40] Haff LA. Improved quantitative PCR using nested primers. PCR Methods Appl 1994;3(6):332–337. doi:10.1101/gr.3.6.332, PMID:7920237.

[41] Robinson JP. Flow cytometry: past and future. Biotechniques 2022;72(4):159–169. doi:10.2144/btn-2022-0005, PMID:35369735.

[42] Batisse C, Marquet J, Greffard A, Fleury-Feith J, Jaurand MC, Pilatte Y. Lectin-based three-color flow cytometric approach for studying cell surface glycosylation changes that occur during apoptosis. Cytometry A 2004;62(2):81–88. doi:10.1002/cyto.a.20094, PMID:15536639.

[43] d'Amati A, Ribatti D, Virgintino D, Errede M. Unveiling Central Nervous System Pericytes: Immunofluorescence Protocol and Confocal Microscopy. Methods Mol Biol 2025;2956:85–96. doi:10.1007/978-1-0716-4706-6_8, PMID:40859077.

[44] Jang C, Chen L, Rabinowitz JD. Metabolomics and Isotope Tracing. Cell 2018;173(4):822–837. doi:10.1016/j.cell.2018.03.055, PMID:29727671.

[45] Souza AL, Patti GJ. A Protocol for Untargeted Metabolomic Analysis: From Sample Preparation to Data Processing. Methods Mol Biol 2021;2276:357–382. doi:10.1007/978-1-0716-1266-8_27, PMID:34060055.

[46] Fiehn O. Metabolomics by Gas Chromatography-Mass Spectrometry: Combined Targeted and Untargeted Profiling. Curr Protoc Mol Biol 2016;114:30.4.1–30.4.32. doi:10.1002/0471142727.mb3004s114, PMID:27038389.

[47] Singh C, Roy-Chowdhuri S. Quantitative Real-Time PCR: Recent Advances. Methods Mol Biol 2016;1392:161–176. doi:10.1007/978-1-4939-3360-0_15, PMID:26843055.

[48] Sauerbrei W, Taube SE, McShane LM, Cavenagh MM, Altman DG. Reporting Recommendations for Tumor Marker Prognostic Studies (REMARK): An Abridged Explanation and Elaboration. J Natl Cancer Inst 2018;110(8):803–811. doi:10.1093/jnci/djy088, PMID:29873743.

[49] Obuchowski NA. Receiver operating characteristic curves and their use in radiology. Radiology 2003;229(1):3–8. doi:10.1148/radiol.2291010898, PMID:14519861.

[50] Akobeng AK. Understanding diagnostic tests 3: Receiver operating characteristic curves. Acta Paediatr 2007;96(5):644–647. doi:10.1111/j.1651-2227.2006.00178.x, PMID:17376185.

[51] Wang P, Li Y, Lv D, Yang L, Ding L, Zhou J, *et al*. Mefatinib as first-line treatment of patients with advanced EGFR-mutant non-small-cell lung cancer: a phase Ib/II efficacy and biomarker study. Signal Transduct Target Ther 2021;6(1):374. doi:10.1038/s41392-021-00773-3, PMID:34719670.

[52] Hassanzad M, Hajian-Tilaki K. Methods of determining optimal cut-point of diagnostic biomarkers with application of clinical data in ROC analysis: an update review. BMC Med Res Methodol 2024;24(1):84. doi:10.1186/s12874-024-02198-2, PMID:38589814.

[53] Mah J, Magari R, Lo KK, Winden N, Xu G. A benefit risk approach in cut-off determination for diagnostic tests. Clin Chim Acta 2024;559:117887. doi:10.1016/j.cca.2024.117887, PMID:38643818.

[54] Martínez Pérez JA, Pérez Martin PS. [ROC curve]. Semergen 2023;49(1):101821. doi:10.1016/j.semerg.2022.101821, PMID:36155265.

[55] Ganesan P, Kulik LM. Hepatocellular Carcinoma: New Developments. Clin Liver Dis 2023;27(1):85–102. doi:10.1016/j.cld.2022.08.004, PMID:36400469.

[56] Alawyia B, Constantinou C. Hepatocellular Carcinoma: a Narrative Review on Current Knowledge and Future Prospects. Curr Treat Options Oncol 2023;24(7):711–724. doi:10.1007/s11864-023-01098-9, PMID:37103744.

[57] Huang C, Xiao X, Zhou L, Chen F, Wang J, Hu X, *et al*. Chinese expert consensus statement on the clinical application of AFP/AFP-L3%/DCP using GALAD and GALAD-like algorithm in HCC. J Clin Lab Anal 2023;37(23-24):e24990. doi:10.1002/jcla.24990, PMID:38063322.

[58] National Health Commission of the People's Republic of China. Clinical Practice Guideline for Primary Liver Cancer (2024 Edition). Xiehe Yi Xue Za Zhi 2024;15(3):532–559. doi:10.12290/xhyxzz.2024-0304.

[59] Minami A, Fujita Y, Shimba S, Shiratori M, Kaneko YK, Sawatani T, *et al*. The sialidase inhibitor 2,3-dehydro-2-deoxy-N-acetylneuraminic acid is a glucose-dependent potentiator of insulin secretion. Sci Rep 2020;10(1):5198. doi:10.1038/s41598-020-62203-8, PMID:32251344.

[60] Wu Q, Ba-Alawi W, Deblois G, Cruickshank J, Duan S, Lima-Fernandes E, *et al*. GLUT1 inhibition blocks growth of RB1-positive triple negative breast cancer. Nat Commun 2020;11(1):4205. doi:10.1038/s41467-020-18020-8, PMID:32826891.

[61] Gupta R, Leon F, Thompson CM, Nimmakayala R, Karmakar S, Nallasamy P, *et al*. Global analysis of human glycosyltransferases reveals novel targets for pancreatic cancer pathogenesis. Br J Cancer 2020;122(11):1661–1672. doi:10.1038/s41416-020-0772-3, PMID:32203219.

[62] Sadeghi F, Kardar GA, Bolouri MR, Nasri F, Sadri M, Falak R. Overexpression of bHLH domain of HIF-1 failed to inhibit the HIF-1 transcriptional activity in hypoxia. Biol Res 2020;53(1):25. doi:10.1186/s40659-020-00293-4, PMID:32503642.

[63] Leviatan Ben-Arye S, Yu H, Chen X, Padler-Karavani V. Profiling Anti-Neu5Gc IgG in Human Sera with a Sialoglycan Microarray Assay. J Vis Exp 2017;125:e56094. doi:10.3791/56094, PMID:28745644.

[64] Dorvignit D, García-Martínez L, Rossin A, Sosa K, Viera J, Hernández T, *et al*. Antitumor and cytotoxic properties of a humanized antibody specific for the GM3(Neu5Gc) ganglioside. Immunobiology 2015;220(12):1343–1350. doi:10.1016/j.imbio.2015.07.008, PMID:26224247.

[65] Lopes AL, Paulino AC, Thaumaturgo MAS, Araújo MS, Caloba P, Kawanishi K, *et al*. Dietary intake of the red meat-derived glycan Neu5Gc fuels colorectal cancer through up-regulation of Wnt signaling pathway. Cancer Lett

2025;616:217598. doi:10.1016/j.canlet.2025.217598, PMID:40023392.

[66] Bashir S, Fezeu LK, Leviatan Ben-Arye S, Yehuda S, Reuven EM, Szabo de Edelenyi F, et al. Association between Neu5Gc carbohydrate and serum antibodies against it provides the molecular link to cancer: French NutriNet-Santé study. BMC Med 2020;18(1):262. doi:10.1186/s12916-020-01721-8, PMID:32962714.

[67] Soulillou JP, Padler-Karavani V. Editorial: Human Antibodies Against the Dietary Non-human Neu5Gc-Carrying Glycans in Normal and Pathologic States. Front Immunol 2020;11:1589. doi:10.3389/fimmu.2020.01589, PMID:32793227.

[68] Rodrigues M, Echigoya Y, Fukada SI, Yokota T. Current Translational Research and Murine Models For Duchenne Muscular Dystrophy. J Neuromuscul Dis 2016;3(1):29–48. doi:10.3233/JND-150113, PMID:27854202.

[69] Crowe KE, Zygmunt DA, Heller K, Rodino-Klapac L, Noguchi S, Nishino I, et al. Visualizing Muscle Sialic Acid Expression in the GNED207VTgGne-/-Cmah-/- Model of GNE Myopathy: A Comparison of Dietary and Gene Therapy Approaches. J Neuromuscul Dis 2022;9(1):53–71. doi:10.3233/JND-200575, PMID:34511508.

[70] Kwon DN, Choi YJ, Cho SG, Park C, Seo HG, Song H, et al. CMP-Neu-5Ac Hydroxylase Null Mice as a Model for Studying Metabolic Disorders Caused by the Evolutionary Loss of Neu5Gc in Humans. Biomed Res Int 2015;2015:830315. doi:10.1155/2015/830315, PMID:26558285.

[71] Samraj AN, Läubli H, Varki N, Varki A. Corrigendum: involvement of a non-human sialic Acid in human cancer. Front Oncol 2014;4:83. doi:10.3389/fonc.2014.00083, PMID:24795860.

[72] Li X, Zhou Y, Li T, Tu X, Zhu S, Wang L, et al. Spatial isotope deep tracing deciphers inter-tissue metabolic crosstalk. Nat Commun 2025;16(1):7934. doi:10.1038/s41467-025-63243-2, PMID:40858577.

[73] MacPherson S, Duncan KD, Goodlett DR, Lum JJ. Strategies for uncovering stable isotope tracing patterns between cell populations. Curr Opin Biotechnol 2023;83:102991. doi:10.1016/j.copbio.2023.102991, PMID:37619527.

[74] Dong W, Rawat ES, Stephanopoulos G, Abu-Remaileh M. Isotope tracing in health and disease. Curr Opin Biotechnol 2022;76:102739. doi:10.1016/j.copbio.2022.102739, PMID:35738210.

[75] Yang JY, Zhang R, Zhang ZR, Li S, Gong DA, Li CH, et al. GFAT1 promotes the progression of hepatocellular carcinoma via enhancing the O-GlcNAcylation of VEZF1. Cell Death Dis 2025;16(1):647. doi:10.1038/s41419-025-07975-5, PMID:40858565.

[76] Zhang X, Zhong Y, Miao Z, Yang Q. Hyaluronic acid promotes hepatocellular carcinoma proliferation by upregulating CD44 expression and enhancing glucose metabolism flux. Int Immunopharmacol 2025;147:114035. doi:10.1016/j.intimp.2025.114035, PMID:39798466.

[77] Liu R, Gou D, Xiang J, Pan X, Gao Q, Zhou P, et al. O-GlcNAc modified-TIP60/KAT5 is required for PCK1 deficiency-induced HCC metastasis. Oncogene 2021;40(50):6707–6719. doi:10.1038/s41388-021-02058-z, PMID:34650217.

[78] Lam C, Low JY, Tran PT, Wang H. The hexosamine biosynthetic pathway and cancer: Current knowledge and future therapeutic strategies. Cancer Lett 2021;503:11–18. doi:10.1016/j.canlet.2021.01.010, PMID:33484754.

[79] Huang HW, Chen CY, Huang YH, Yeh CT, Wang CS, Chang CC, et al. CMAHP promotes metastasis by reducing ubiquitination of Snail and inducing angiogenesis via GM-CSF overexpression in gastric cancer. Oncogene 2022;41(2):159–172. doi:10.1038/s41388-021-02087-8, PMID:34716430.

[80] Xiao-Jie L, Ai-Mei G, Li-Juan J, Jiang X. Pseudogene in cancer: real functions and promising signature. J Med Genet 2015;52(1):17–24. doi:10.1136/jmedgenet-2014-102785, PMID:25391452.

[81] Bousquet PA, Sandvik JA, Edin NFJ, Krengel U. Addendum to: Hypothesis: Hypoxia induces de novo synthesis of NeuGc gangliosides in humans through CMAH domain substitute. Biochem Biophys Res Commun 2022;587:166. doi:10.1016/j.bbrc.2021.11.074, PMID:34865824.

[82] Silva-Filho AF, Sena WLB, Lima LRA, Carvalho LVN, Pereira MC, Santos LGS, et al. Glycobiology Modifications in Intratumoral Hypoxia: The Breathless Side of Glycans Interaction. Cell Physiol Biochem 2017;41(5):1801–1829. doi:10.1159/000471912, PMID:28376491.

[83] Wu Z, Wu J, Zhao Q, Fu S, Jin J. Emerging roles of aerobic glycolysis in breast cancer. Clin Transl Oncol 2020;22(5):631–646. doi:10.1007/s12094-019-02187-8, PMID:31359335.

[84] Yin J, Hashimoto A, Izawa M, Miyazaki K, Chen GY, Takematsu H, et al. Hypoxic culture induces expression of sialin, a sialic acid transporter, and cancer-associated gangliosides containing non-human sialic acid on human cancer cells. Cancer Res 2006;66(6):2937–2945. doi:10.1158/0008-5472.CAN-05-2615, PMID:16540641.